Chapter 5

STUDIES ON A SERIES OF CHIRAL COPPER BASED ORGANIC-INORGANIC HYBRID COMPOUNDS (OIHCs)

Abstract

This chapter describes syntheses of copper chloride based OIHCs, having two different general formula A_2CuCl_4 (**Part A**) and $ACuCl_4$ (**Part B**). In the **Part A** we have synthesized seven OIHCs using monofunctional chiral OACSs, which investigated for possible solid-solid phase transition using thermal analyses and single crystal XRD study. TG/DTA measurements have shown salts have interesting decomposition pathways in which organic amine and/or hydrochloride gas compete for the 'first' loss. DSC measurement represent reversible solid-solid phase transitions at HT correspond to thermochromic behavior. In case of [(*R*)- and (*S*)-ethyl benzilinium]$_2CuCl_4$ (**15** and **16**) solid-solid phase transitions observed at LT. To confirm this phase transition we have collected single crystal XRD data at different temperature. Single crystal XRD examined on these compounds reflects that they crystallized monoclinic chiral space group *C2* at 296 K and adopts monoclinic space group $P2_1$ at 150 K. Thus single crystal XRD proved solid-solid phase transition around 237.7 K for compounds **15**, and **16** due to structural change.

In **Part B** we have synthesized two OIHCs using bifunctional chiral OACSs. These are investigated for thermal analyses, crystal structure and magnetic properties. DSC measurements on chiral OIHCs: [(*R*)-propane-1,2-diammonium]$CuCl_4$ (**18**) and [(*S*)-propane-1,2-diammonium]$CuCl_4$ (**19**) have shown reversible solid-solid phase transition with endothermic peak around 404.8 K while heating and exothermic peak around 389.0 K while cooling. Single crystal XRD analyses for compounds **18** and **19** showed it crystallized in orthorhombic chiral space group $P2_12_12_1$ with unit cell dimensions a = 7.1756(3) Å, b = 7.9615(3) Å, c = 16.0075(6) Å, V = 914.49(6) Å^3, Z = 4 and a = 7.1744(3) Å, b = 7.9453(4) Å, c = 16.0098(7) Å, V = 912.60(7) Å^3, Z = 4 respectively. Temperature dependence magnetic measurements on compounds **18** and **19** using SQUID magnetometer display field-induced metamagnetism.

5.1 Introduction

When we construct magnets using chiral molecules, chirality must be controlled not only in the molecular structure, but in the entire crystal structure as well [1]. However, in most cases, structural chirality did not sufficiently relate to the magnetic properties, because of isotropic electronic configurations of the constituents. When magnet is characterized by chiral structure there is a possibility that it may have a chiral spin structure and the magnet may display asymmetric magnetic anisotropy magneto-chiral dichroism (MChD). MChD effect depends on the magnitude of the magnetic moments. It is advantageous to make fully chiral molecule-based magnets, which are expected to exhibit a strong MChD effect. Furthermore, chirality may make magnetic molecules crystallize in the polar point group, which is required for ferroelectricity [2,3]. Therefore, the synthesis and properties of chiral magnets are of continuous, increasing interest due to their potential important applications as in magneto optical application [4]. The chiral molecule-based magnets supply a new approach to the designable multifunctional materials.

Therefore this chapter deals with utilization of chiral ligand, as an OACSs and is divided in two parts.

1) **Part A:** Use of monofunctional chiral OACSs. This part describe preparation, thermal analyses, reversible structural phase transition, thermochromic behavior and single crystal X-ray structure of copper (II) based OIHCs with general formula A_2CuCl_4, incorporating.
2) **Part B:** Used bifunctional (**18** and **19**) chiral OACSs. We describe crystal structure and magnetic behavior in OIHCs having general formula $ACuCl_4$. Thermochromic behavior of these compounds is also investigated.

Part A

5A.2 Experimental

5A.2.1 *Materials and Methods*

All chemicals and solvents used were of analytical grade reagents. (*R*)- and (*S*)-methyl benzyl amine, (*R*)- and (*S*)-4-chloro methyl benzyl amine, (*R*)- and (*S*)-ethyl benzyl amine, (*S*)-2-butyl amine and copper (II) chloride (Aldrich); conc. hydrochloric acid (qualigens) and ethyl alcohol (Baroda chemicals) were used without any further purification.

5A.2.2 Syntheses of OIHCs: (A_2CuCl_4)

A general methodology of OIHCs preparation/syntheses is mentioned in scheme-II.

Scheme-II

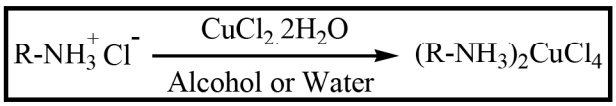

[Where, R = 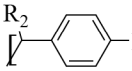 {R_1 = H and R_2 = CH_3 (*R*) (**11**), R_1 = H and R_2 = CH_3 (*S*) (**12**), R_1 = Cl and R_2 = CH_3 (*R*) (**13**), R_1 = Cl and R_2 = CH_3 (*S*) (**14**), R_1 = H and R_2 = C_2H_5 (*R*) (**15**), and R_1 = Cl and R_2 = C_2H_5 (*S*) (**16**)} and (*S*)-$CH_3CH_2CH(CH_3)$- (**17**)]

In actual process, compounds [(*R*)- and (*S*)-methyl benzilinium]$_2CuCl_4$ (**11** and **12**) were synthesized in nitrogen environment by dissolving the appropriate amounts (2:1 ratio) 0.5 mL (476.0 mg, 3.928 mmol) of (*R*)- and (*S*)-methyl benzilinium chloride and 335.0 mg (1.964 mmol) of $CuCl_2.2H_2O$ in acidified distilled water. Subsequently the solutions were heated at 373 K for 3 - 4 hours. Evaporation of water was carried out using vacuum pump. The precipitates were rinsed with ether and recrystallized in ethanol by slow evaporation technique. After the one week dark green colored crystals of compounds **11**, **12** (sugar like) were obtained. The greenish

yellow colored crystals obtained for compounds **13**, **14** (plate like); **15**, **16** and **17** (needle like).

Yield: **11**, **12** (80 %); **13**, **14** (50 %); **15**, **16** (55 - 60 %) and **17** (40 %)

5A.3 Results and Discussions

5A.3.1 General Discussion

The XRD measurements on $[C_6H_5(CH_2)_nNH_3]_2CuCl_4$ (n = 1, 2, 3) and (n-$C_4H_9NH_3)_2CuCl_4$ revealed two-dimensional layered structure consisting of $CuCl_4^{2-}$ inorganic sheets formed by corner-sharing copper chloride octahedra; successive inorganic sheets are interleaved by two layers of organic ammonium molecule [5,6]. The XRD studies for $(C_6H_5CH_2NH_3)_2CuCl_4$ by Daoud *et al.* and (n-$C_4H_9NH_3)_2CuCl_4$ by chiarella shows it crystallize in orthorhombic space group *Pbca* [7,8]. Single crystal XRD measurement on $(C_6H_5CH_2NH_3)_2CuCl_4$ by Polyakov *et al.* have found it crystallized in *Pbca* at 100 K and in *Cmca* above the 370 K [9]. Thus by changing the position of amino group in OACSs, compounds **11**, **12**, **13**, **14**, **15** and **16** crystallized in monoclinic chiral space group *C2*, isolated structure of $CuCl_4^{2-}$ at RT. The compounds **15** and **16** show the solid-solid structural phase transition at 150 K, crystallized in monoclinic chiral space group $P2_1$. While compound **17** crystallized in orthorhombic chiral space group $P2_12_12_1$ forming zigzag chain of $CuCl_4^{2-}$ with semicoordinate bond for compound **17**.

5A.3.2 FT-IR Spectra

Analytical data for the OIHCs are given below.

11: FT-IR (KBr) 2946 (vs), 2656 (m), 1593 (vs), 1564 (s), 1494 (vs), 1454 (vs), 1386 (vs), 1370 (m), 1334 (w) 1314 (m), 1288 (m), 1222 (vs), 1161 (m), 1083 (s), 1058 (s), 1029 (m), 970 (s), 918 (m), 766 (vssh), 749 (m), 697 (vssh), 536 (vssh) and 476 (m) cm^{-1}.

12: FT-IR (KBr) 3054 (vs), 2656 (m), 1593 (vs), 1564 (s), 1493 (vs), 1454 (vs), 1386 (vs), 1370 (m), 1334 (w), 1314 (m), 1288 (m), 1222 (vs), 1161 (m), 1083 (s),

1058 (s), 1029 (m), 970 (s), 918 (m), 766 (vssh), 749 (m), 697 (vssh), 537 (vssh) and 476 (m) cm^{-1}.

13: FT-IR (KBr) 3053 (vs), 2924 (vs), 2607 (m), 1615 (vs), 1495 (vs), 1454 (w), 1416 (m), 1386 (s), 1305 (w), 1280 (w), 1224 (s), 1167 (w), 1096 (vs), 1014 (s), 975 (w), 829 (vssh), 771 (s), 719 (w), 642 (m), 539 (s) and 418 (w) cm^{-1}.

14: FT-IR (KBr) 3051 (vs), 2909 (s), 2715 (m), 2657 (m), 2605 (m), 1656 (w), 1590 (s), 1497 (vs), 1452 (m), 1418 (m), 1387 (ssh), 1365 (w), 1341 (w), 1306 (m), 1277 (w), 1224 (m), 1167 (w), 1113 (w), 1096 (s), 1066 (m), 1014 (s), 970 (s), 884 (m), 827 (vssh), 770 (s), 720 (m), 668 (m), 640 (m), 538 (s) and 417 (w) cm^{-1}.

15: FT-IR (KBr) 3040 (vs), 2662 (m), 1594 (vs), 1495 (vs), 1455 (s), 1380 (s), 1331 (w), 1215 (w), 1167 (w), 1000 (w), 1067 (m), 1008 (w), 965 (w), 916 (w), 815 (w), 763 (ssh), 736 (w), 697 (vssh), 579 (m), 537 (s) and 468 (w) cm^{-1}.

16: FT-IR (KBr) 3040 (vs), 2661 (m), 1594 (vs), 1495 (vs), 1456 (s), 1380 (s), 1331 (w), 1215 (w), 1167 (w), 1000 (w), 1068 (w), 1008 (w), 965 (w), 916 (w), 816 (w), 763 (ssh), 736 (w), 698 (vssh), 580 (m), 538 (s) and 468 (w) cm^{-1}.

17: FT-IR (KBr) 3123 (vs), 2975 (vs), 2622 (m), 2529 (m), 1599 (vs), 1493 (vs), 1484 (vs), 1393 (ssh), 1289 (w), 1212 (s), 1134 (m), 1007 (s), 968 (m), 895 (w), 810 (w), 776 (m) and 418 (s) cm^{-1}.

The vibrational measurements for OIHCs were recorded in the range of 4,000 - 400 cm^{-1} at RT. FT-IR show asymmetric stretching bands of N-H (-NH_3^+ group) shifted at 3224 - 2600 cm^{-1} (this result in broad feature centered around 3000 cm^{-1}) indicates breaking of continuous series of hydrogen bond. However, an intense band around 2657 cm^{-1} can be resolved into two features at 2715 cm^{-1} and 2605 cm^{-1}. The feature at 2715 cm^{-1} assigned be to the Fermi resonance processes corresponding to combination bands of N-H (-NH_3^+ group) deformation modes and N-H (-NH_3^+ group) rocking modes [10]. The other N-H (-NH_3^+ group) deformation and rocking modes were observed around 1656 cm^{-1} and 1066 cm^{-1}. The vibration occurred at 1225 cm^{-1} (aliphatic) and 1306 cm^{-1} (aromatic) due to C-N stretching. Other bands which provide vital information about the *para*-substituent on aromatic ring due to aromatic

C-H out of plane deformation signify two hydrogen adjacent positions at 826 cm^{-1}. FT-IR spectra of compounds **11**, **14**, **15** and **17** are shown in Figure 5A.1.

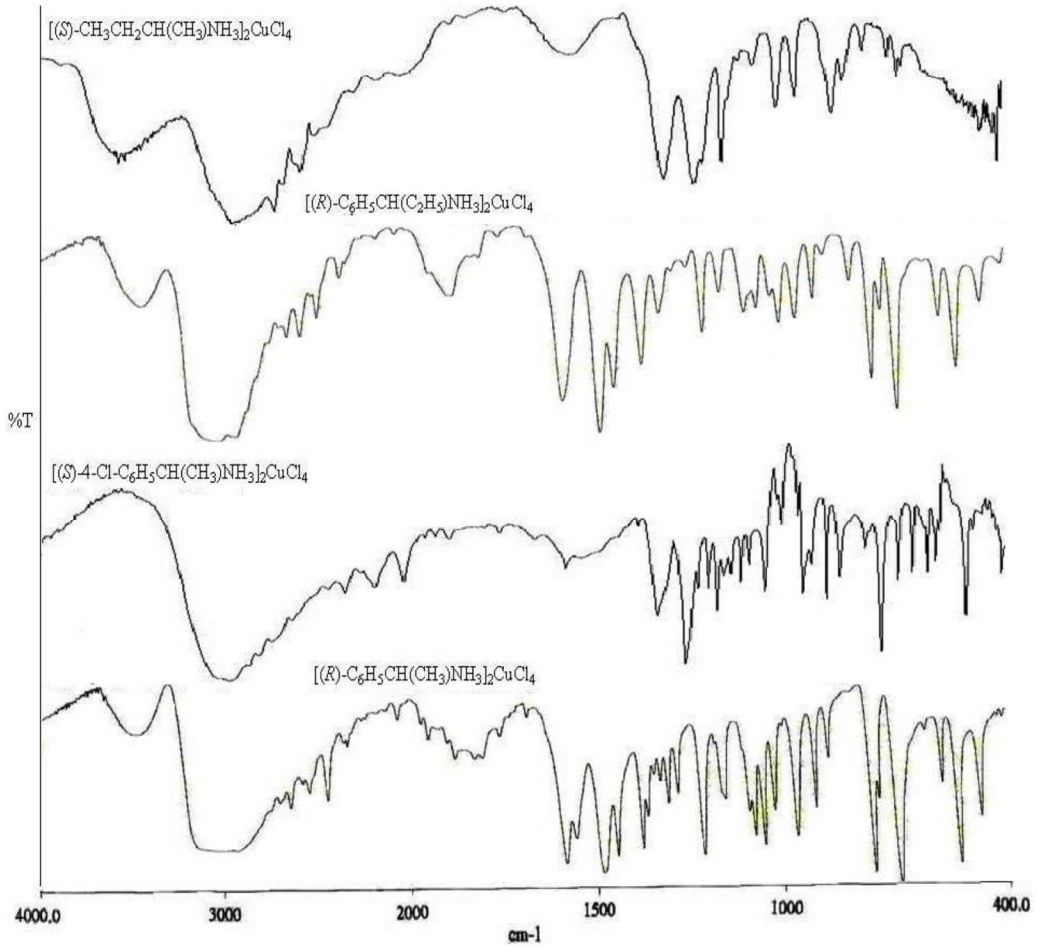

Figure 5A.1 FT-IR spectra of compounds **11**, **14**, **15** and **17**.

5A.3.3 Elemental Analyses

The elemental analyses were consistent with the formulae A_2CuCl_4. *Anal.* Ref. sulfanilamide: Found (calc.) %; C, 41.85 (41.81); H, 4.68 (4.65); N, 15.26 (16.25). [(*R*)-$C_6H_5CH(CH_3)NH_3]_2CuCl_4$ (**11**)**:** Found (calc.) %; C, 42.72 (42.42); H, 5.34 (5.44); N, 6.22 (6.32). [(*S*)-$C_6H_5CH(CH_3)NH_3]_2CuCl_4$ (**12**)**:** Found (calc.) %; C, 42.72 (43.01); H, 5.34 (4.94); N, 6.22 (6.84). [(*R*)-4-Cl-$C_6H_4CH(CH_3)NH_3]_2CuCl_4$ (**13**)**:** Found (calc.) %; C, 37.05 (37.05); H, 4.24 (4.10); N, 5.40 (5.35). [(*S*)-4-Cl-$C_6H_4CH(CH_3)NH_3]_2CuCl_4$ (**14**)**:** Found (calc.) %; C, 37.05 (37.24); H, 4.24 (4.34); N, 5.40 (5.54). [(*R*)-$C_6H_5CH(C_2H_5)NH_3]_2CuCl_4$ (**15**)**:** Found (calc.) %; C, 45.25 (44.95); H, 5.86 (5.26); N, 5.86 (5.76). [(*S*)-$C_6H_5CH(C_2H_5)NH_3]_2CuCl_4$ (**16**)**:** Found (calc.) %;

C, 45.25 (45.84); H, 5.86 (5.91); N, 5.86 (5.60). [(*S*)-$CH_3CH_2CH(CH_3)NH_3]_2CuCl_4$ (**17**)**:** Found (calc.) %; C, 27.16 (27.24); H, 6.79 (6.99); N, 7.92 (7.94).

5A.3.4 Thermal Analyses

5A.3.4.1 Thermo gravimetry/Differential Thermal Analysis (TG/DTA)

TG/DTA of layered OIHCs was performed on the powdered compounds. Figure 5A.2 show the thermal analyses of compounds **11**, **13**, **14**, **15** and **17**. Compounds **11**, **12** and **14** follow similar degradation pathways as compared to compounds **13**, **15**, **16** and **17**, as tabulated below.

$[(R)\text{-}C_6H_5CH(CH_3)NH_3]_2CuCl_4$

Temp. 541.3 K ↓ $2(R)\text{-}C_6H_5CH(CH_3)NH_2HCl$
Loss = 70.10 % (theory)
Loss = 73.64 % (found)

$CuCl_2$

Temp. 822.5 K ↓ Cl_2
Loss = 15.78 % (theory)
Loss = 17.41 % (found)

Cu
14.13 % (theory)
8.96 % (found)

$[(S)\text{-}C_6H_5CH(CH_3)NH_3]_2CuCl_4$

Temp. 542.5 K ↓ $2(S)\text{-}C_6H_5CH(CH_3)NH_2HCl$
Loss = 70.10 % (theory)
Loss = 73.74 % (found)

$CuCl_2$

Temp. 821.4 K ↓ Cl_2
Loss = 15.78 % (theory)
Loss = 16.99 % (found)

Cu
14.13 % (theory)
9.27 % (found)

$[(R)\text{-}4\text{-}Cl\text{-}C_6H_4CH(CH_3)NH_3]_2CuCl_4$

Temp. 553.6 K ↓ $2(R)\text{-}4\text{-}Cl\text{-}C_6H_4CH(CH_3)NH_2HCl$
Loss = 74.07 % (theory)
Loss = 74.15 % (found)

$CuCl_2$

Temp. 856.1 K ↓ $CuCl_2$
Loss = 25.93 % (theory)
Loss = 24.96 % (found)

Complete loss

$[(S)\text{-}4\text{-}Cl\text{-}C_6H_4CH(CH_3)NH_3]_2CuCl_4$

Temp. 547.6 K ↓ $2(S)\text{-}4\text{-}Cl\text{-}C_6H_4CH(CH_3)NH_2HCl$
Loss = 74.07 % (theory)
Loss = 77.36 % (found)

$CuCl_2$

Temp. 822.8 K ↓ Cl_2
Loss = 13.68 % (theory)
Loss = 14.24 % (found)

Cu
12.25 % (theory)
8.41 % (found)

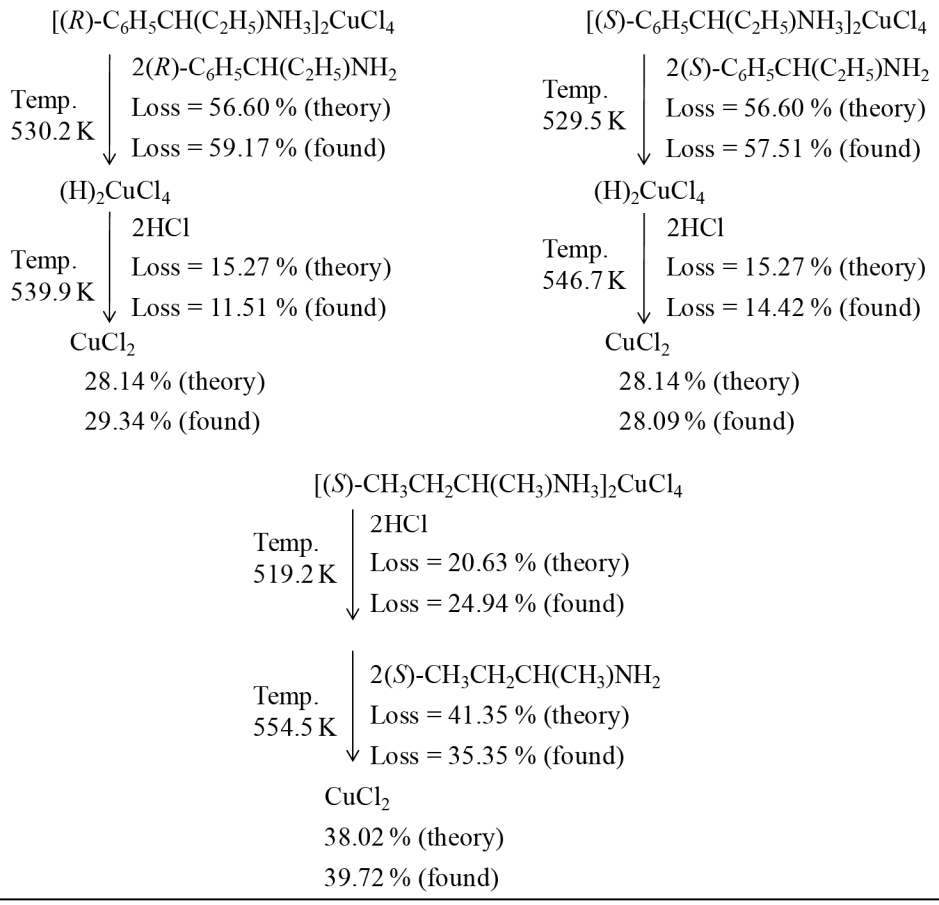

DTA of compound **11** shows endothermic peak at 541.3 K due to thermal decomposition. Calculation of weight loss at this temperature comes very close to the evaporation of two moles of (*R*)-methyl benzilinium chloride molecule per formula unit. Second weight loss at 822.5 K is due to the evaporation of Cl_2 molecule per formula unit. This decomposition path of compound **11** is very similar to compounds **12** and **14**. While in compounds **13**, **15**, **16** and **17** thermal decomposition path are totally different. DTA of compounds **13**, **15**, **16** and **17** shows endothermic peak at 444 K (**13**) and exothermic peaks at 530.0 K (**15**, **16**) and at 519.2 K (**17**) are the characteristic for thermal decomposition. Here, compound **13** shows the complete weight loss (chlorine molecule loses along with Cu) after the decomposition of organic ammonium chloride. Compounds **15**, and **16** shows the initial decomposition of two moles of (*R*)- and (*S*)-ethyl benzyl amine. At HT, above 530.0 K it loses further two moles of hydrochloride and converts to $CuCl_2$ which is stable up to 773 K. In case of compound **17** two moles of hydrochloride are lost in initial heating instead of (*S*)-2-butyl ammonium chloride. (*S*)-2-butyl amine loses afterwards leaving behind

$CuCl_2$ above 554.5 K. The DTA of all compounds except compound **17** have shown the peak before the degradation temperature which are characteristics for the solid-liquid phase transition (see Figure 5A.2). The exothermic peaks observed in DTA for compounds **15**, **16** and **17** at 530.0 K and at 519.2 K respectively. Normally exothermic peaks are observed due to crystallization or desolvation/dehydration. Thus, thermal analyses represented different thermo chemical reactions operating in these compounds are essential for cleavage of bond or rearrangement of ligand.

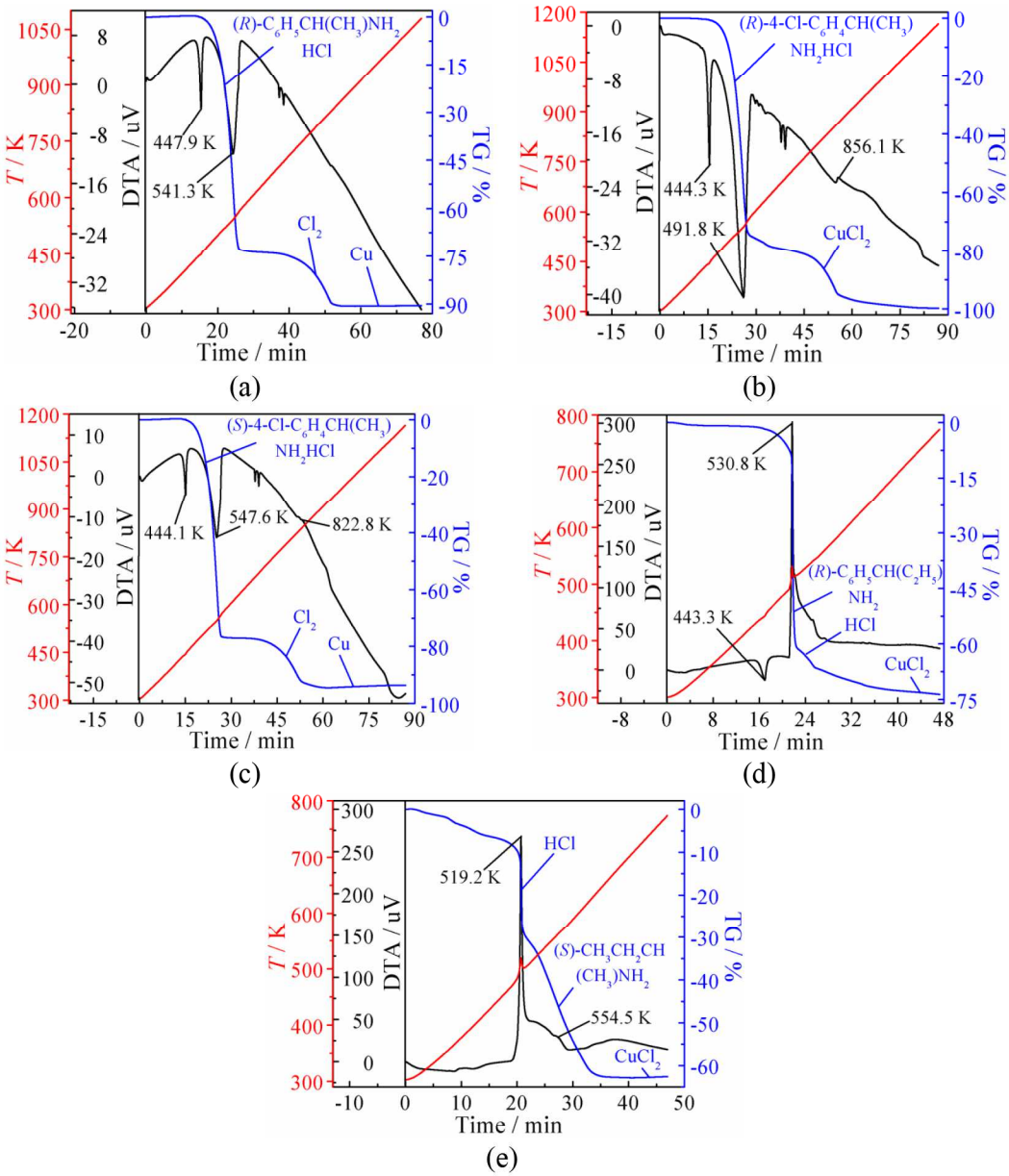

Figure 5A.2 Thermo gravimetric curve for compounds **11** (a); **13** (b); **14** (c); **15** (d) and **17** (e).

The degradation pathways of these OIHCs in comparison with their only ligands have different degradation pathways. The decomposition paths of (*R*)- and (*S*)-methyl benzilinium chloride are very similar to (*R*)- and (*S*)-ethyl benzilinium chloride, where organic amine and hydrochloride are lost at same temperature. In case of (*R*)- and (*S*)-4-chloro methyl benzilinium chloride and (*S*)-2-butyl ammonium chloride one mole of hydrochloride lost in initial heating then organic amine. For details of decomposition paths in OACSs see chapter 3.3.5.

5A.3.4.2 Differential Scanning Calorimetry (DSC)

To confirm our different degradation pathway and exothermic behavior of DTA we carried out DSC on all OACSs and their complexes from 173 K to their degradation temperature. We observed the reversible solid-solid phase transition for all compounds after the formation of complexes. The compounds **11**, **12**, **13**, **14** and **17** have shown one endothermic peak at 406.10 K (-6.36 J g^{-1}), 406.34 K (-4.48 J g^{-1}), 404.16 K (-0.87 J g^{-1}), 405.08 K (-1.61 J g^{-1}) and 379.50 K (-99.48 J g^{-1}) respectively while heating, and one exothermic peak at 383.50 K (1.63 J g^{-1}), 383.64 K (1.09 J g^{-1}), 393.49 K (0.33 J g^{-1}), 388.31 K (0.59 J g^{-1}) and 347.46 K (96.92 J g^{-1}) respectively while cooling. These peaks are characteristics for solid-solid phase transition [Figure 5A.3 (a), (b) and (e)]. The compounds **15** and **16** shows two endothermic peaks at 237.81 K (-12.02 J g^{-1}), 404.72 K (-3.88 J g^{-1}) and 237.71 K (-14.32 J g^{-1}), 403.78 K (-5.36 J g^{-1}) respectively while heating, and two exothermic peaks at 223.37 K (13.02 J g^{-1}), 390.27 K (1.81 J g^{-1}) and 223.78 K (14.20 J g^{-1}), 389.60 K (2.26 J g^{-1}) respectively while cooling which are characteristics for solid-solid phase transitions as shown in Figure 5A.3 (c) and (d). Details of phase changes are given in Table 5A.1. These solid-solid transitions are reversible in nature and can be repeated in many cycles without any observable change in peak. To confirm this solid-solid phase change we have heated the compounds up to their transition temperature in open atmosphere through the heating plate. As per our expectation we observed change in color (green color ↔ dark brown for compounds **11**, **12** and yellow-green ↔ yellow-brown for compounds **13**, **14**, **15**, **16**) after heating-cooling cycles as shown in Figure 5A.4. Compound **17** did not show any color change up to the transition temperature. The green or yellow-green color at RT is observed when Cl-Cu-Cl trans angle is around 147º (or above). The color changes to dark brown or yellow-brown as this

angle decreases. If the colour becomes green or yellow-green then the angle increases. So in this case we believe that Cl-Cu-Cl trans angle changes drastically below 147º. It has shown that color change is associated with a relaxation of the stereochemistry from a square-planar (or square pyramidal or square bi-pyramidal) geometry towards a tetrahedral geometry [11]. The phenomenon of thermochromism in copper halide salts appears to be strongly associated with the dynamics of the organic counter ions. The change of color from green to brown (or vice versa) is reported in literature but no data is available for yellow-green to yellow-brown for copper (II) complex [12].

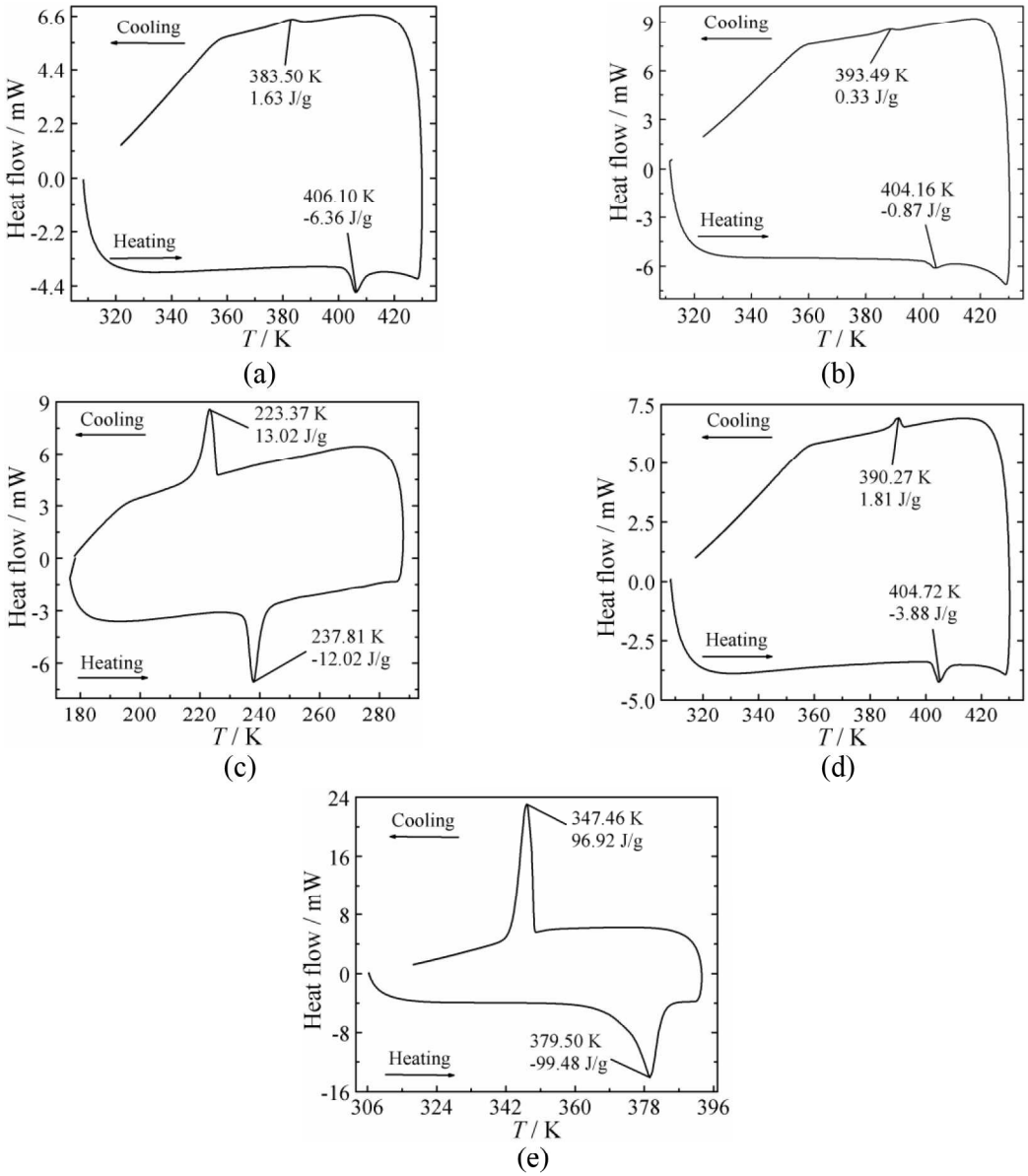

Figure 5A.3 DSC plot for compounds **11** (a); **13** (b); **15** at LT (c), at HT (d) and **17** (e), showing the reversible transitions.

Table 5A.1 DSC chart of OIHCs

Compounds	Phase Transition			
	Heating		Cooling	
	Temperature [K]	Enthalpy [J g^{-1}]	Temperature [K]	Enthalpy [J g^{-1}]
11	406.10	-6.36	383.50	1.63
12	406.34	-4.48	383.64	1.09
13	404.16	-0.87	393.49	0.33
14	405.08	-1.61	388.31	0.59
15	237.81	-12.02	223.37	13.02
	404.72	-3.88	390.27	1.81
16	237.71	-14.32	223.78	14.20
	403.78	-5.36	389.60	2.26
17	379.50	-99.48	347.46	96.92

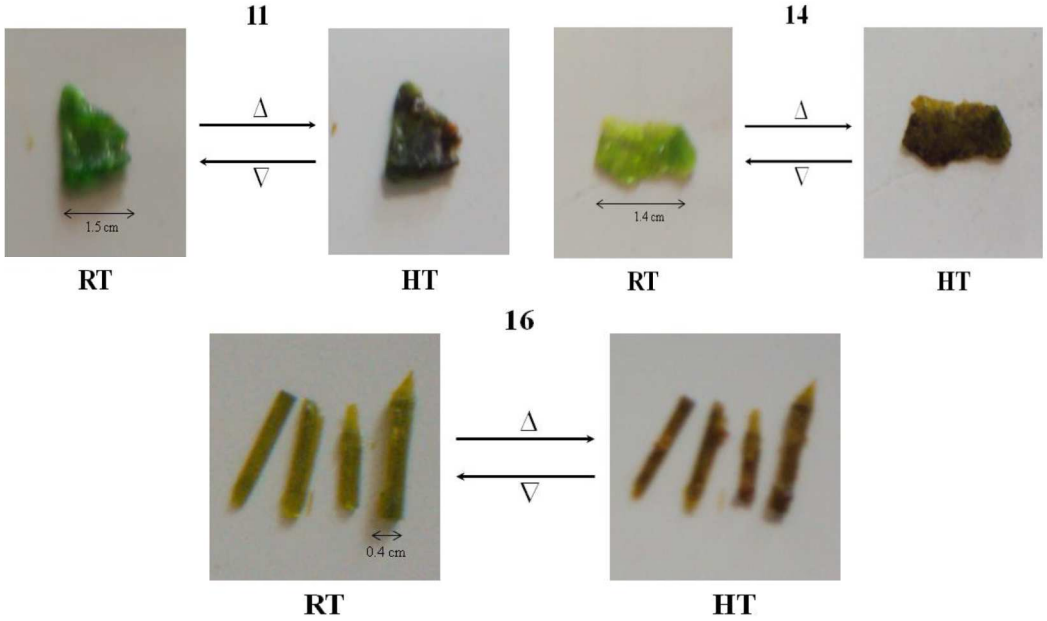

Figure 5A.4 Thermochromic behaviors in crystal of compounds **11**, **14** and **16**, shows complete reversible color.

5A.3.5 Crystal Structure

Crystallographic data collection parameters and refinement data for compounds **11**, **12**, **13**, **14**, **15**, **16** and **17** are illustrated in Table 5A.2, 5A.3 and 5A.4. Figure 5A.5 shows the asymmetric unit of compounds **11**, **13**, **15** and **17**.

Table 5A.2 Crystallographic data and structure refinements for compounds **11**, **12**, **13** and **14** at RT

Compounds	**11**	**12**	**13**	**14**
Empirical formula	$C_{16}H_{24}Cl_4CuN_2$	$C_{16}H_{24}Cl_4CuN_2$	$C_{16}H_{22}Cl_6CuN_2$	$C_{16}H_{22}Cl_6CuN_2$
Formula weight	449.71	449.71	518.61	518.60
T (K)	293	293	296	293
Wavelength (Å)	0.71073	0.71073	0.71073	0.71073
Crystal system	Monoclinic	Monoclinic	Monoclinic	Monoclinic
Space group	*C2*	*C2*	*C2*	*C2*
a (Å)	10.567(3)	10.582(3)	10.016(7)	10.245(2)
b (Å)	7.253(2)	7.257(2)	7.266(5)	7.307(2)
c (Å)	13.926(4)	13.940(3)	15.540(2)	15.634(5)
β (°)	95.99(3)	96.04(2)	91.90(2)	91.21(2)
V (Å^3)	1061.5(5)	1064.5(5)	1130.2(3)	1170.0(5)
Z	2	2	2	2
D_{calc} (Mg/m^3)	1.407	1.403	1.524	1.472
Crystal size (mm^3)	0.30×0.28×0.24	0.31×0.29×0.25	0.29×0.27×0.22	0.26×0.24×0.16
F(000)	693	462	526	526
2θ range (°)	2.94 - 28.93	2.94 - 28.79	1.31 - 27.00	3.43 - 28.98
Index ranges	-13 ≤ h ≤ 14, -9 ≤ k ≤ 9, -9 ≤ l ≤ 18	-14 ≤ h ≤ 13, -9 ≤ k ≤ 7, -10 ≤ l ≤ 18	-12 ≤ h ≤ 9, -9 ≤ k ≤ 9, -19 ≤ l ≤ 19	-12 ≤ h ≤ 13, -9 ≤ k ≤ 9, -16 ≤ l ≤ 21
Reflections collected	2266	2263	4187	2682
Independent reflections	1848 [R_{int} = 0.0185]	1688 [R_{int} = 0.0209]	2215 [R_{int} = 0.0338]	2049 [R_{int} = 0.0248]
Completeness to θ = 25.00°	99.8 %	99.9 %	97.5 %	99.7 %
Goodness-of-fit on F^2	1.031	0.974	1.076	0.987
Data / restraints / parameters	1848 / 1 / 105	1688 / 1 / 105	2215 / 1 / 116	2049 / 1 / 114
Final R indices [I>2σ(I)]	*R1* = 0.0324, w*R2* = 0.0685	*R1* = 0.0346, w*R2* = 0.0633	*R1* = 0.0329, w*R2* = 0.1067	*R1* = 0.0443, w*R2* = 0.0756
R indices (all data)	*R1* = 0.0404, w*R2* = 0.0750	*R1* = 0.0438, w*R2* = 0.0689	*R1* = 0.0385, w*R2* = 0.1263	*R1* = 0.0678, w*R2* = 0.0892

Table 5A.3 Crystallographic data and structure refinements for compounds **15** and **16** at RT and at LT

Compounds	**15**	**16**	**15'**	**16'**
Empirical formula	$C_{18}H_{28}Cl_4CuN_2$	$C_{18}H_{28}Cl_4CuN_2$	$C_{18}H_{28}Cl_4CuN_2$	$C_{18}H_{28}Cl_4CuN_2$
Formula weight	477.76	477.76	477.76	477.76
T (K)	296	296	150	150
Wavelength (Å)	0.71073	0.71073	0.71073	0.71073
Crystal system	Monoclinic	Monoclinic	Monoclinic	Monoclinic
Space group	*C2*	*C2*	$P2_1$	$P2_1$
a (Å)	11.099(3)	11.119(2)	10.700(2)	10.696(2)
b (Å)	7.287(2)	7.282(2)	7.306(2)	7.308(3)
c (Å)	14.673(3)	14.655(3)	14.267(2)	14.268(4)
β (°)	98.19(2)	98.15(2)	98.41(2)	98. 42(2)
V (Å^3)	1174.5(4)	1174.9(5)	1103.3(3)	1103.2(4)
Z	2	2	2	2
D_{calc} (Mg/m^3)	1.351	1.350	1.438	1.438
Crystal size (mm^3)	0.46×0.30×0.14	0.37×0.14×0.01	0.31×0.20×0.08	0.31×0.20×0.08
F(000)	494	494	494	494
2θ range (°)	3.36 - 33.73	3.35 - 20.00	2.89 - 33.73	1.92 - 25.68
Index ranges	-17 ≤ h ≤ 17, -11 ≤ k ≤ 10, -22 ≤ l ≤ 22	-13 ≤ h ≤ 13, -8 ≤ k ≤ 7, -17 ≤ l ≤ 16	-16 ≤ h ≤ 16, -11 ≤ k ≤ 10, -22 ≤ l ≤ 22	-13 ≤ h ≤ 11, -8 ≤ k ≤ 8, -17 ≤ l ≤ 15
Reflections collected	7383	3121	14791	4374
Independent reflections	4390 [R_{int} = 0.0313]	1630 [R_{int} = 0.1146]	6883 [R_{int} = 0.0313]	3484 [R_{int} = 0.0219]
Completeness to θ = 33.73°	98.5 %	98.5 %	99.5 %	99.2 %
Goodness-of-fit on F^2	0.921	1.019	0.978	1.012
Data / restraints / parameters	4390 / 1 / 114	1630 / 1 / 114	6883 / 1 / 250	3484 / 1 / 250
Final R indices [I>2σ(I)]	*R1* = 0.0432, w*R2* = 0.0934	*R1* = 0.0573, w*R2* = 0.1388	*R1* = 0.0339, w*R2* = 0.0678	*R1* = 0.0345, w*R2* = 0.0756
R indices (all data)	*R1* = 0.1241, w*R2* = 0.1225	*R1* = 0.0815, w*R2* = 0.1576	*R1* = 0.0443, w*R2* = 0.0716	*R1* = 0.0440, w*R2* = 0.0797

Table 5A.4 Crystallographic data and structure refinements for compound **17** at RT

Empirical formula	$C_8H_{24}Cl_4CuN_2$	Crystal size (mm^3)	0.46×0.16×0.13
Formula weight	353.63	$F(000)$	732
T (K)	296	2θ range (°)	1.93 - 28.69
Wavelength (Å)	0.71073	Index ranges	-7 ≤ h ≤ 9, -18 ≤ k ≤ 15, -22 ≤ l ≤ 19
Crystal system	Orthorhombic	Reflections collected	13098
Space group	$P2_12_12_1$	Independent reflections	4029 [R_{int} = 0.0247]
a (Å)	7.108(2)	Completeness to θ = 28.69°	99.7 %
b (Å)	13.850(2)	Goodness-of-fit on F^2	1.045
c (Å)	16.290(3)	Data / restraints / parameters	4029 / 0 / 136
V ($Å^3$)	1603.7(4)	Final R indices [$I>2\sigma(I)$]	$R1$ = 0.0303, w$R2$ = 0.0695
Z	4	R indices (all data)	$R1$ = 0.0396, w$R2$ = 0.0731
D_{calc} (Mg/m^3)	1.465		

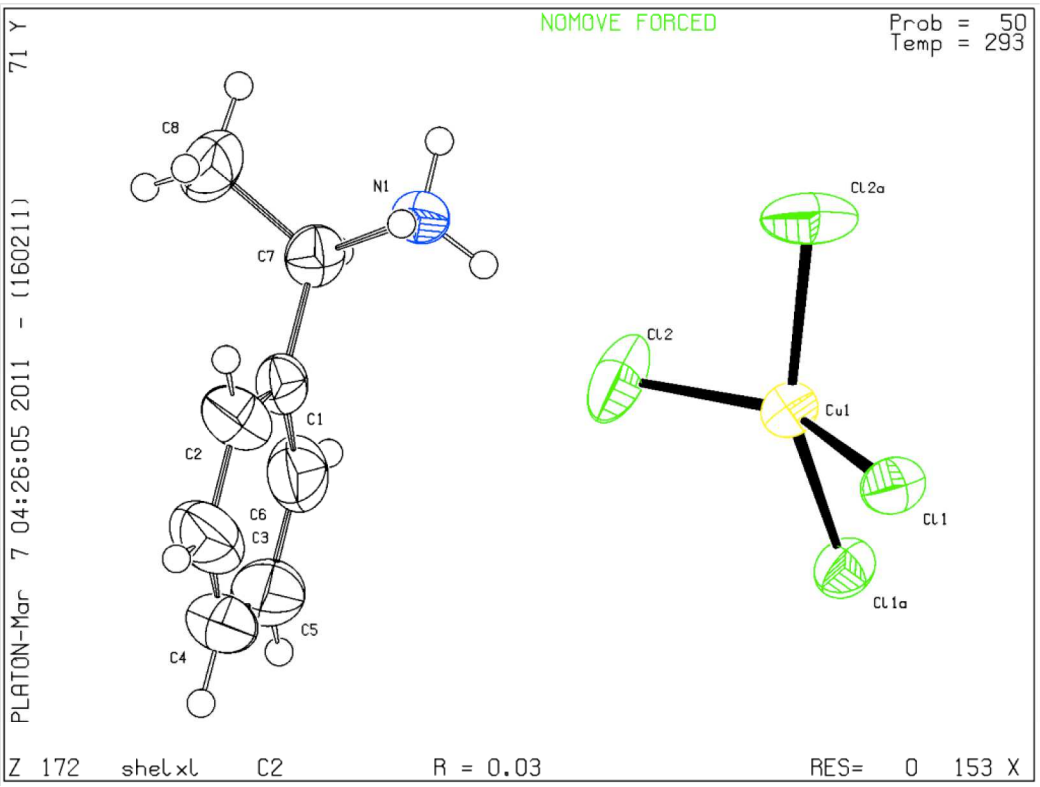

(a)

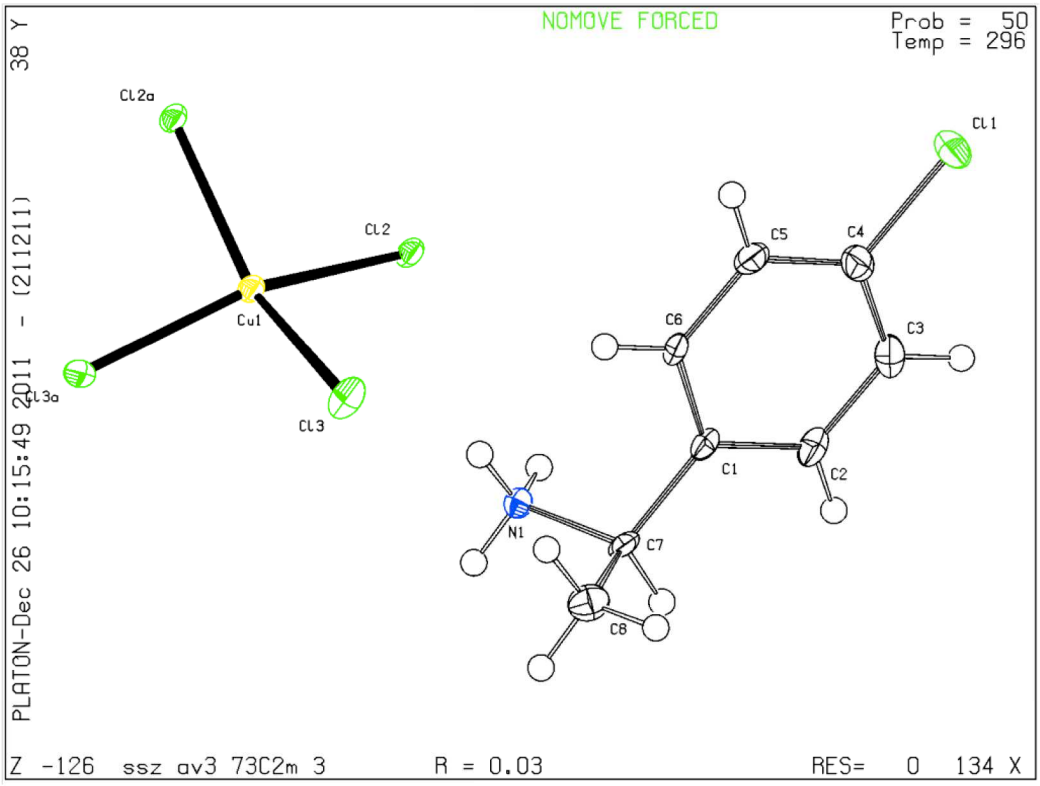
NOMOVE FORCED
Prob = 50
Temp = 296
38 Y
PLATON-Dec 26 10:15:49 2011 - (211211)
Cl2a
Cl2
Cu1
Cl3a
Cl3
Cl1
C5
C4
C6
C3
C1
C2
N1
C7
C8
Z -126 ssz av3 73C2m 3
R = 0.03
RES= 0 134 X

(b)

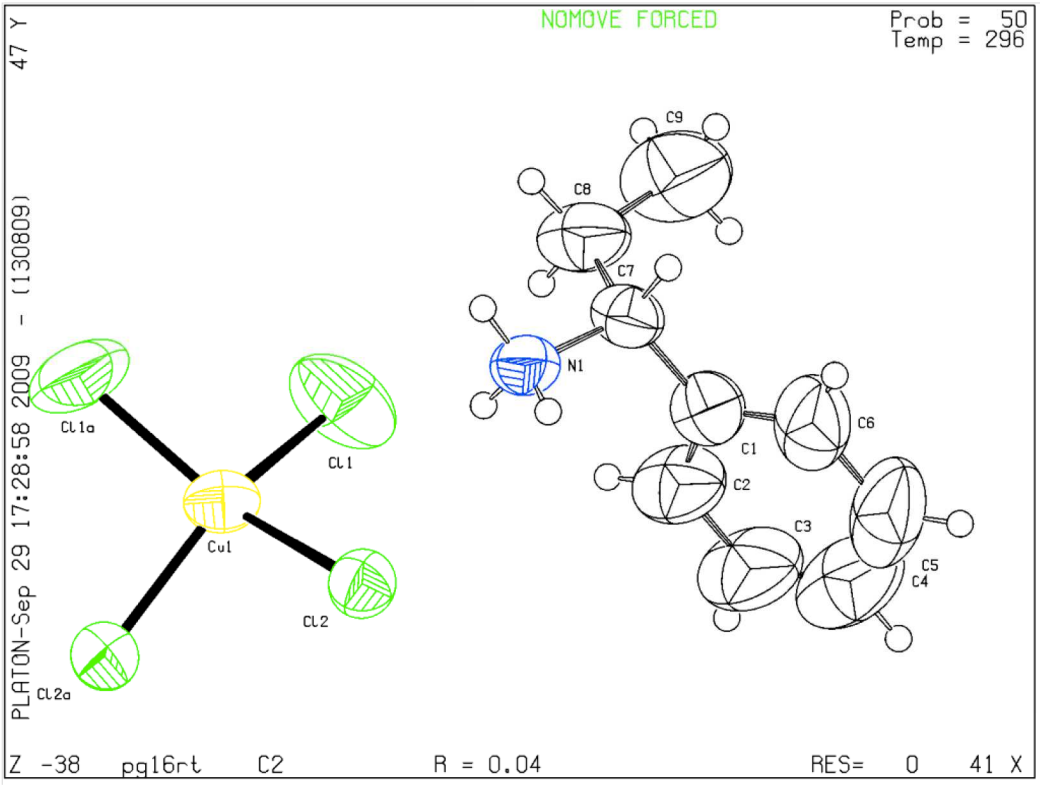
NOMOVE FORCED
Prob = 50
Temp = 296
47 Y
PLATON-Sep 29 17:28:58 2009 - (130809)
C9
C8
C7
N1
C1
C6
C2
C3
C5
C4
Cl1a
Cl1
Cu1
Cl2
Cl2a
Z -38 pg16rt C2
R = 0.04
RES= 0 41 X

(c)

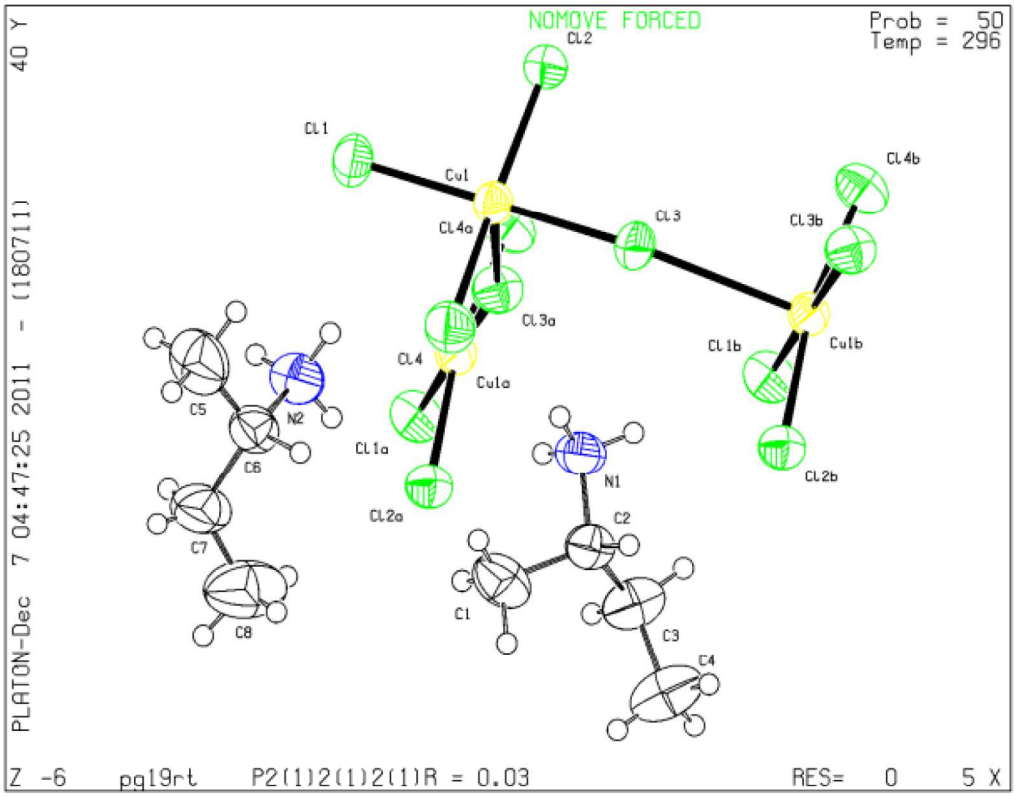

(d)

Figure 5A.5 Molecular view of compounds **11** (a); **13** (b); **15** (c) and **17** (d), at RT with labeling scheme, displacement ellipsoids are drawn at the 50 % probability level.

Single crystal XRD on compounds **11**, **12**, **13**, **14**, **15** and **16** showed that they crystallize in monoclinic chiral space group *C2* while compound **17** crystallize in orthorhombic chiral space group $P2_12_12_1$ at RT. Former six of the seven crystal structures consisted of isolated, highly distorted tetrahedral geometry (nearest to intermediate between tetrahedral and square-planar geometry) of $CuCl_4^{2-}$ anions. While the later one (**17**) forms zigzag chains of $CuCl_4^{2-}$ ions with semicoordinate bond which are perpendicular to each other.

Literature have shown copper chloride salts of $[C_6H_5(CH_2)_nNH_3]_2CuCl_4$ (n = 1, 2, 3) and (n-butyl ammonium)$_2CuCl_4$ consists of two-dimensional layered structure of $CuCl_4^{2-}$, where each layer is comprised of an extended network of corner-sharing metal halide octahedra. Thus in the present series of the compounds the geometries of $CuCl_4^{2-}$ are differ distinctly due to three reasons (a) steric (b) hydrogen bonding effects (c) chirality insertion, to explain the notable difference between motions of the two anions. Any substituent on the α-carbon makes hindrance to the layered structure.

The crystallographic data are given in Table 5A.2, 5A.3 and 5A.4. The dianions of compounds **11**, **12**, **13**, **14**, **15** and **16** display isolated, highly distorted tetrahedral geometry with average Cl-Cu-Cl trans angle 147º - 155º. These dianions are intercalated by OACs and stabilized by weak force (van der Waals) and hydrogen bonding interaction. The two ions (cations and anions) are held together by N-H···Cl interaction with bond angle 116º - 179º and distance 3.179(3) Å - 3.294(4) Å. The data summarizing these contacts are listed in Table 5A.5. Three types of N-H···Cl hydrogen bonds are observed in all the compounds at RT. Later five (compounds **13**, **14**, **15**, **16** and **17**) of the seven crystal structures consisted of N-H···Cl and C-H···Cl interactions. Similarity, we have not observed any such type (C-H···Cl) of interaction for compounds **11** and **12**. There are a few unsystematic in the geometric nature of N-H···Cl interaction. The N-H···Cl angles do not correlate with the variations in the N-H···Cl distances. For example, compounds have almost similar N-H···Cl distances but the N-H···Cl angles are differing. Direct comparison of the relative importance of N-H···Cl and C-H···Cl interactions in this set of structures is difficult to do, on the basis of structural motifs. The change in N-H···Cl angles for compounds **13** and **14** is not possible to make a direct comparison (Table 5A.5).

Table 5A.5 Crystal parameter for compounds **11**, **12**, **13**, **14**, **15**, **16**, **15'**, **16'** and **17**

Compounds	Cu-Cl [Å]	Cu-Cu Dist. [Å] Inter	Cu-Cu Dist. [Å] Intra	Cl-Cl Dist. [Å] Terminal	Cl-Cu-Cl Angle[°]	N···Cl Dist. [Å]	N-H···Cl Angle[°]
11	2.264(1)	13.926(1)	6.408(1)	10.694(2)	152.2(1)	3.180(3)	157.9(2)
	2.239(1)					3.228(3)	151.9(2)
						3.235(3)	132.4(2)
12	2.269(1)	13.940(1)	6.416(1)	10.700(2)	152.1(1)	3.179(4)	157.9(2)
	2.239(1)					3.240(3)	152.9(2)
						3.230(4)	132.3(2)
13	2.264(1)	15.540(2)	6.187(2)	12.356(2)	150.0(1)	3.180(3)	158.0(2)
	2.245(1)					3.220(3)	146.7(2)
						3.195(3)	122.9(2)
14	2.259(1)	15.634(1)	6.292(1)	12.467(3)	150.3(1)	3.191(5)	162.5(3)
	2.238(2)					3.239(4)	151.9(3)
						3.216(4)	130.6(3)
15	2.263(2)	14.673(1)	6.638(1)	11.385(2)	147.1(1)	3.236(3)	164.3(2)
	2.211(2)					3.198(3)	162.3(2)
						3.213(3)	136.5(2)
16	2.263(4)	14.655(3)	6.646(1)	11.378(7)	147.1(1)	3.235(6)	166.4(4)
	2.206(4)					3.202(7)	163.9(4)
						3.218(7)	137.4(4)

15'	2.286(2)	14.267(1)	6.224(1)	11.112(1)	154.5(1)	3.230(2)	172(3)
	2.256(2)				148.4(1)	3.224(2)	168(3)
	2.253(2)					3.252(2)	155(2)
	2.240(2)					3.291(2)	153(2)
						3.258(2)	128(2)
16'	2.286(1)	14.268(1)	6.2231(6)	11.111(2)	154.46(4)	3.294(4)	161.3(5)
	2.254(1)				148.33(4)	3.289(5)	160.5(4)
	2.242(1)					3.241(5)	155.6(10)
						3.233(5)	147.4(4)
						3.259(5)	120.4(3)
17	2.871(1)	8.939(2)	5.106(1)	5.059(1)	179.4(1)	3.268(3)	178.4(2)
	2.297(1)				169.4(1)	3.245(3)	126.2(2)
	2.295(1)					3.182(3)	116.0(2)
	2.273(1)						
	2.271(1)						

The studied structures demonstrated that there is a competition between the non-covalent interactions. In contrast, only N-H···Cl hydrogen bonds are observed for compounds **11**, **12** Figure 5A.6 (a). Two different N-H···Cl and C-H···Cl interaction are seen for compounds **13** and **14**, and **15** and **16** at RT Figure 5A.6 (b), 5A.7 (a). At LT two N-H···Cl and C-H···Cl interaction also observed compounds **15** and **16** [Figure 5A.7 (b)]. A closer look at the structural data measured for compounds **15**, **16** at RT and **15'**, **16'** at LT revealed comparable unit cell parameters in the monoclinic system. As could be expected the unit cell of compounds **15** and **16** at RT are slightly larger [1174.45(9) versus 1103.33(5) $Å^3$]. However, the two data sets belong to different chiral space groups namely, *C2* and $P2_1$. A comparison of the selected metric parameters associated with the $CuCl_4^{2-}$ anion and the chiral part of the cation (Table 5A.5) revealed significant contraction (ca. 0.15 Å) of Cu-Cl bond distances. Also, the Cl-Cu-Cl bonds exhibit changes: one Cl-Cu-Cl trans angles is contracted by 7.5° [154.49(2) versus 147.12(5)°]. In contrast cation exhibits very little difference. Whereas the torsion angles associated with the chiral carbon atom exhibit small changes the rest of the bond distances and angles are comparable. At RT benzylic C-C torsion angle was found around -59º for all (*R*)- and (*S*)-ethyl benzilinium cations. When viewed from the side (*i.e.* parallel to the plane of the phenyl group) molecules [C(1)-C(7)-C(8)-C(9)] adopt an unusual J-shaped conformation. But it showed some of the (*R*)- and (*S*)-ethyl benzilinium cations give the C-C single bond rotations at LT and adopted benzylic C-C torsion angle 179º at LT for **15'**, **16'**. The resulting *trans* conformation for propyl ammonium fragment [C(1)-C(7)-C(8)-C(9)] is depicted in Table 5A.6. These are stabilized by van der Waals interaction between the OACs

therefore organic layer slight tilt in compounds **15'** and **16'**. Compounds have torsion angles -59º and 179º for compounds **15'** and **16'** at LT. Based on the comparison, we suggest that the choice of space group at different temperatures is determined by the fluxional nature of the $[CuCl_4]^{2-}$ anion. It appeared that anion transitions from a highly distorted tetrahedral geometry at RT towards a see-saw geometry when the temperature is lowered.

Structural data interpretation have revealed $CuCl_4^{2-}$ anions accumulate for compound **17** and becomes distorted square pyramidal geometry (Cl-Cu-Cl angles are close to 169º and 179.5º) which forms zigzag chains with semicoordinate bond these are perpendicular to each other Figure 5A.8. The structural examination illustrates two N-H···Cl and C-H···Cl interaction are observed for compound **17** at RT. The better geometry of Cu^{2+} ion is specified as 4+1+1 or even 4+1 coordination and the layers are nearly sliced in $(CuCl_4^{2-})_n$ zigzag chain. The extreme elongation of one semicoordinate bond allowed the accommodation of chiral (*S*)-2-butyl ammonium cations between the zigzag chains. The ammonium groups need to fit into the "holes" formed by terminal and bridging halogen within the distorted Perovskite-type structure without rest of the molecule interfering with the sheets.

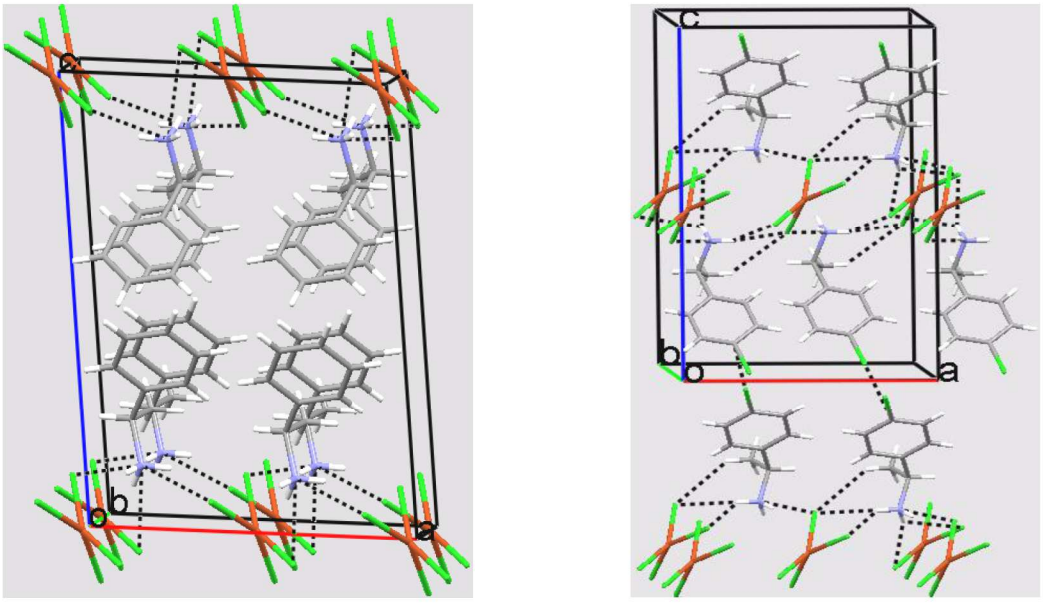

(a) (b)

Figure 5A.6 The monoclinic structures for compounds **11** (a) and **14** (b), viewed down along the *b*-axis, showing isolated structure of $CuCl_4^{2-}$ and bonding scheme in the compounds.

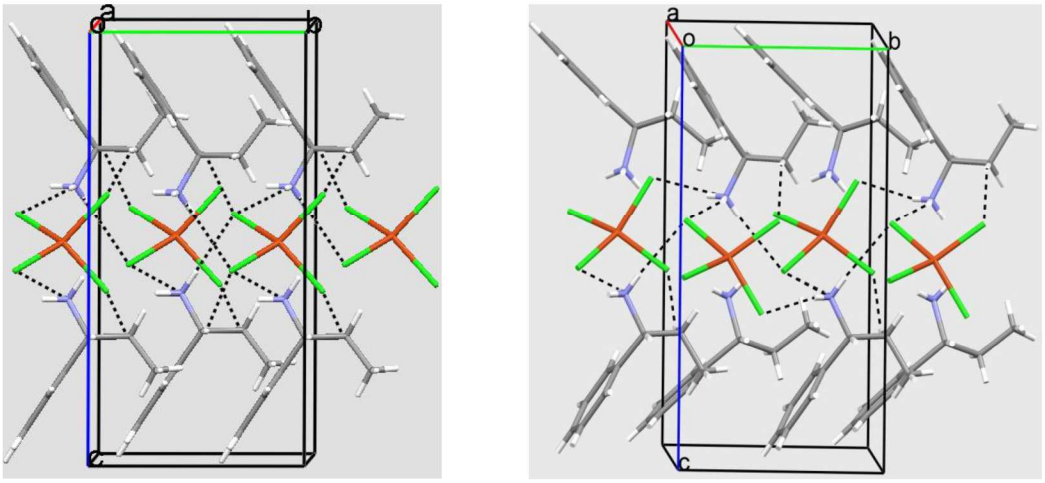

(a) (b)

Figure 5A.7 The monoclinic structures for compounds **15** (**a**) and **15'** (**b**), viewed down along the *a*-axis, showing isolated structure of $CuCl_4^{2-}$ and bonding scheme in the compounds.

Table 5A.6 Torsion angles [°] for compounds **15**, **16**, **15'** and **16'**

Torsion Angle	15	16	15'	16'
C(1)-C(7)-C(8)-C(9)	-59.6(5)	-61.5(11)	-59.4(3)	-59.0(5)
N(1)-C(7)-C(8)-C(9)	176.0(4)	175.8(8)	177.12(19)	177.2(4)
N(2)-C(16)-C(17)-C(18)			56.7(3)	56.2(5)
C(10)-C(16)-C(17)-C(18)			178.67(19)	178.4(4)

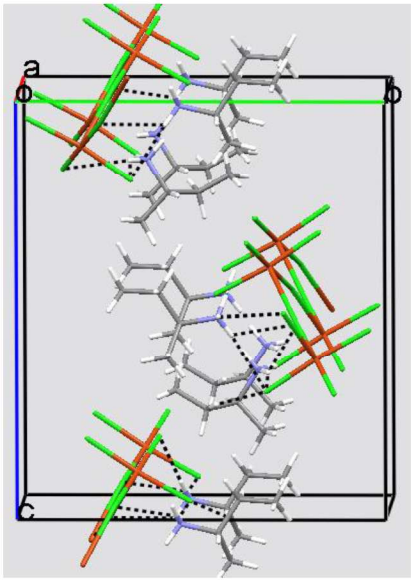

Figure 5A.8 The orthorhombic structures for compound **17** viewed down along the *a*-axis, illustrate zigzag chain structure of $CuCl_4^{2-}$ and bonding scheme in the compound.

CCDC No. 817150, 817151, 817530, 817531, 817838, 883058 and 882748 contains the crystallographic data for the compounds **11**, **12**, **13**, **14**, **15**, **16** and **17** respectively. These data can be obtained free of charge via http://www.ccdc.cam.ac.uk/conts/retrieving.html, or from the Cambridge Crystallographic Data Centre, 12 Union Road, Cambridge CB2 1EZ, UK; fax: (+44) 1223 336 033; or e-mail: deposit@ccdc.cam.ac.uk.

5A.4 Conclusion

- We have synthesized seven OIHCs having general formula A_2CuCl_4 by choosing organic (chiral) monofunctional molecule.
- Thermal studies on these OIHCs confirm that organic ammonium chloride was first loss for compounds **11**, **12**, **13**, **14** and organic amine was first loss for compounds **15**, **16**. On the other hand hydrochloride gas was first loss for compound **17**.
- DSC measurements showed solid-solid phase transition observed only at HT. The solid-solid phase transition at HT is accompanied by the reversible change in colors from green ↔ dark brown for compound **11** and **12**; and yellow-green ↔ yellow-brown for **13**, **14**, **15** and **16**, indicating the thermochromic behavior. While in case of compounds **15** and **16** reversible solid-solid phase transitions also observed at LT.
- At 296 K compounds **15** and **16** crystallized isostructurally [monoclinic, *C2* (chiral space group)] with compounds **11**, **12**, **13** and **14**, and at 150 K it adopts monoclinic, $P2_1$ (chiral space group). While compound **17** crystallized in orthorhombic space group $P2_12_12_1$ at 296 K.
- The two data sets for compounds **15** and **16** belong to monoclinic chiral space groups *C2* and $P2_1$ at 296 K and 150 K respectively. In these structures N-H···Cl and C-H···Cl interactions play a significant role.
- Single crystal XRD displayed that isolated highly distorted tetrahedral geometry of $CuCl_4^{2-}$ were observed for all OIHCs, except compound **17**. Compound **17** has zigzag chain of $CuCl_4^{2-}$ with semicoordinate bond which are perpendicular to each other.

References

[1] G. L. J. A. Rikken, E. Raupach, *Nature* **1997**, *390*, 493-494.

[2] N. A. Hill, A. Filippetti, *J. Mag. Mag. Mater.* **2002**, *242-245*, 976-979.

[3] Z. -G. Gu, X. -H. Zhou, Y. -B. Jin, R. -G. Xiong, J. -L. Zuo, X. -Z. You, *Inorg. Chem.* **2007**, *46*, 5462-5464.

[4] M. A. Ahmed, M. A. Gabal, F. A. Radwan, *J. Mater. Sci.* **2003**, *38*, 3677-3682.

[5] J. -K. Kang, C. Jeon, *Synth. Met.* **1995**, *71*, 1879-1880.

[6] Z. -L. Xiao, H. -Z. Chen, M. -M. Shi, G. Wu, R. -J. Zhou, Z. -S. Yang, M. Wang, B. -Z. Tang, *Mater. Sci. Engg. B* **2005**, *117*, 313-316.

[7] A. Dupas, K. Le Dang, J. -P. Renard, P. Veillet, A. Daoud, R. Perret, *J. Chem. Phys.* **1976**, *65*, 4099-4102.

[8] F. Chiarella, Growth and Characterization of Films of Perovskite Based Organic-Inorganic Hybrid Materials for Electronics, Università Degli Studi Di Napoli Federico II, **2005**, 1-110.

[9] A. O. Polyakov, A. H. Arkenbout, J. Baas, G. R. Blake, A. Meetsma, A. Caretta, P. H. M. van Loosdrecht, T. T. M. Palstra, *Chem. Mater.* **2012**, *24*, 133-139.

[10] E. K. Gibson, J. M. Winfield, K. W. Muir, R. H. Carr, A. Eaglesham, A. Gavezzotti, D. Lennon, *Phys. Chem. Chem. Phys.* **2010**, *12*, 3824-3833.

[11] C. Zanchini, R. D. Willett, *Inorg. Chem.* **1990**, *29*, 3027-3030.

[12] V. K. Belsky, V. Fernandez, V. E. Zavodnik, I. Diaz, J. L. Martinez, *Crystallogr. Rep.* **2001**, *46*, 779-785.

Part B

5B.2 Experimental

5B.2.1 *Materials and Methods*

All chemicals were used of reagent grade. (*R*)- and (*S*)-1,2-diamino propane dihydrochloride, copper (II) chloride (Aldrich) Co. purity 99 + % and conc. hydrochloric acid were purchased from Qualigens. They were used without any further purification.

5B.2.2 Syntheses of OIHCs: ($ACuCl_4$)

A general methodology of OIHCs preparation is shown in scheme-II.

Scheme-II

$$^{-}Cl\ ^{+}H_3N\text{-}R\text{-}NH_3^{+}\ Cl^{-} \xrightarrow[\text{Alcohol or Water}]{CuCl_2.2H_2O} (H_3N\text{-}R\text{-}NH_3)CuCl_4$$

[Where, R = (*R*)- -$CH(CH_3)CH_2$- (**18**), (*S*)- -$CH(CH_3)CH_2$- (**19**)]

In actual process, compounds **18** and **19** were synthesized in the presence of nitrogen atmosphere by dissolving the appropriate amounts (1:1 ratio) 100.0 mg (0.680 mmol) of (*R*)- and (*S*)-1,2-diamino propane dihydrochloride and 116.0 mg (0.680 mmol) of copper (II) chloride in acidified distilled water. Subsequently, solution was heated at 373 K for 3 - 4 hours and discarded all the water using vacuum pump. The residue was recrystallized with acidified water. After 3 - 4 weeks yellow-green color shining rectangular prism like suitable for single crystals were formed.

Yield: 55 %

5B.3 Results and Discussions

5B.3.1 General Discussion

XRD data were obtained monoclinic space group $P2_1/b$ for $[NH_3(CH_2)_2NH_3]CuCl_4$ by Birrell *et al.* (1972). The orthorhombic space group *Pnma*

for $[NH_3(CH_2)_3NH_3]CuCl_4$ by Phelps *et al.* [1,2]. The compounds **18** and **19** were crystallized in orthorhombic chiral space group $P2_12_12_1$. The Cu-Cl bonds in the coordination sphere average 2.295(3) Å, 2.294(1) Å and 2.2601(4) Å, while the longer semi-coordinate distances are 2.882(3) Å, 2.946(1) Å and 2.3157(5) Å for the $[NH_3(CH_2)_2NH_3]CuCl_4$, $[NH_3(CH_2)_3NH_3]CuCl_4$, and compounds **18** and **19** salts respectively. The bridging Cu-Cl-Cu angles 165.70(4)° and 159.75(3)° are nonlinear for $[NH_3(CH_2)_3NH_3]CuCl_4$, and compounds **18** and **19**, yielding the typical corrugated sheet structure. The ammonium group of $[NH_3(CH_2)_2NH_3]CuCl_4$ and $[NH_3(CH_2)_3NH_3]CuCl_4$ forms terminal halogen configuration (N-H···Cl hydrogen bond interaction by two terminal and one bridged chloride) with the adjacent layer, giving corresponding interlayer Cu···Cu distance of 8.124(3) Å, and 9.123(3) Å respectively. The $-NH_3^+$ group of (*R*)- and (*S*)-1,2-diammonium propane cation formed bifurcated N-H···Cl hydrogen bond with two chlorine (one free and one terminal), with interlayer Cu···Cu distance of 8.0138(4) Å. Thus in compounds **18** and **19** interlayer Cu···Cu is about 0.08(3) Å and 1.08(3) Å close together than $[NH_3(CH_2)_2NH_3]CuCl_4$ and $[NH_3(CH_2)_3NH_3]CuCl_4$. Due to hydrogen bonding with the organic chains the layers are puckered. The N-H···Cl distances range from 3.210(2) Å to 4.170(2) Å, 3.213(3) Å to 3.360(3) Å and 3.1618(14) Å to 3.5720(18) Å for the $[NH_3(CH_2)_2NH_3]CuCl_4$, $[NH_3(CH_2)_3NH_3]CuCl_4$, and **18** and **19** salts respectively.

The magnetic examination for layered structure $[NH_3(CH_2)_2NH_3]CuCl_4$ and $[NH_3(CH_2)_3NH_3]CuCl_4$ have shown typical antiferromagnetic behavior below 31.5 K and 13.5 K [2,3]. The magnetic coupling is determined by the coordination environment and configuration of Cu^{2+} ions. It is obvious that the hydrogen bonding pattern of ammonium group with terminal chlorine, which always tilts the position of $CuCl_4^{2-}$ along the axis and bonding with bridging chlorine always forcing the alternating layer chlorine atoms out of the plane, leading to decreases super exchange pathway through the two chlorides between interlayer copper. The super exchange interaction through the two chlorides between interlayer coppers typically decreases due to tilted position of $CuCl_4^{2-}$. The bridging chlorine bond angle seems to play an important role in controlling the magnetic coupling to be ferromagnetic or antiferromagnetic. Generally, bend Cu-Cl-Cu bond angle is unfavorable for the ferromagnetic coupling between d_Z^2 and d_{XZ} of metal [4]. The average bond angle of compounds **18** and **19** [159.75(3) Å] is much smaller than that of

$[NH_3(CH_2)_3NH_3]CuCl_4$ [165.70(4) Å] [2]. So, the classical antiferromagnetic properties are expected for compounds **18** and **19**. The Cu-Cl-Cu bond angle [159.75(3) Å] of compounds **18** and **19** may be exactly around the critical value require for making the overall coupling change from an antiferromagnetic to ferromagnetic state. This is the region compounds **18** and **19** display intrachain antiferromagnetic properties at a low field but ferromagnetic properties at a high field.

5B.3.2 FT-IR Spectra

FT-IR spectra were recorded in the range of 4,000 - 400 cm^{-1} for compounds **18** and **19** as shown in Figure 5B.1. Analytical data for the compounds are given below.

18: FT-IR (KBr) 3442 (s), 3021 (vs), 1722 (w), 1556 (s), 1494 (vs), 1402 (s), 1354 (m), 1307 (m), 1215 (m), 1148 (m), 1055 (s), 1021 (ssh), 970 (m), 861 (m), 806 (m), 676 (w), 482 (m) and 433 (m) cm^{-1}.

19: FT-IR (KBr) 3441 (m), 3297 (vs), 3022 (vs), 1831 (w), 1558 (vs), 1496 (vs), 1402 (s), 1354 (m), 1215 (m), 1149 (m), 1055 (s), 1022 (ssh), 971 (m), 862 (m), 806 (m), 677 (w), 483 (m) and 435 (m) cm^{-1}.

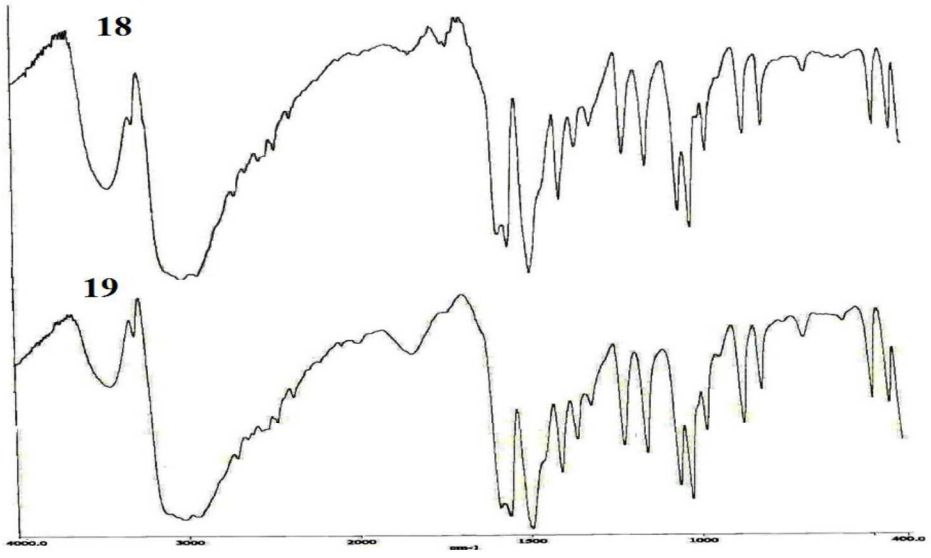

Figure 5B.1 FT-IR spectra of compounds **18** and **19**.

The broad band FT-IR absorption spectra in both enantiomers (*R*)- and (*S*)-1,2-diammonium propane dichloride for N-H ($-NH_3^+$ group) stretching vibrations are observed at 3250 cm^{-1} and 2600 cm^{-1} due to the continuous series of overlapping band,

combination band and overtone band. These broad bands disappear and shifted with sharpening at 3021 cm^{-1} indicating the formation of compounds **18** and **19**. The amine salts of compounds **18** and **19** were characterized by strong triplet bands at 3021 cm^{-1} due to N-H stretching bands of $-NH_3^+$ ions (cf. the C-H stretching bands in this region) and bending vibrations at 1556 cm^{-1}. The feature at 2550 cm^{-1} are assigned Fermi resonance processes corresponding to combination bands of N-H ($-NH_3^+$ group) deformation modes and N-H ($-NH_3^+$ group) rocking modes [5]. The bands at 1494 cm^{-1} and 1055 cm^{-1} are assigned N-H ($-NH_3^+$ group) deformation and rocking respectively. Vibration spectra also observed at 1054 cm^{-1} and 1021 cm^{-1} due to aliphatic C-N stretching.

5B.3.3 Elemental Analyses

The elemental analyses were consistent with the formulae $ACuCl_4$. *Anal.* Ref. sulfanilamide: Found (calc.) %; C, 41.85 (41.81); H, 4.68 (4.65); N, 15.26 (16.25). $[(R)\text{-}NH_3CH(CH_3)CH_2NH_3]_2CuCl_4$ (**18**)**:** Found (calc.) %; C, 12.49 (12.79); H, 4.51 (4.26); N, 9.84 (9.95). $[(S)\text{-}NH_3CH(CH_3)CH_2NH_3]_2CuCl_4$ (**19**)**:** Found (calc.) %; C, 12.74 (12.79); H, 4.41 (4.26); N, 9.98 (9.95).

5B.3.4 Thermal Analyses

5B.3.4.1 Thermogravimetry/differential thermal analysis (TG/DTA)

Figure 5B.2 show the thermal analyses of compounds **18** and **19**. The compounds **18** and **19** show the similar degradation pathway as tabulated below.

$[(R)\text{-}1,2\text{-}H_3NCH(CH_3)CH_2NH_3]CuCl_4$	$[(S)\text{-}1,2\text{-}H_3NCH(CH_3)CH_2NH_3]CuCl_4$
Temp. 483.3 K ↓ $(R)\text{-}1,2\text{-}H_2NCH(NH_3)CH_2NH_2$	Temp. 481.9 K ↓ $(S)\text{-}1,2\text{-}H_3NCH(CH_2)CH_2NH_2$
Loss = 26.33 % (theory)	Loss = 26.33 % (theory)
Loss = 16.18 % (found)	Loss = 15.04 % (found)
$(H)_2CuCl_4$	$(H)_2CuCl_4$
Temp. 599.7 K ↓ $2HCl + Cl_2$	Temp. 596.0 K ↓ $2HCl + Cl_2$
Loss = 51.13 % (theory)	Loss = 51.13 % (theory)
Loss = 58.34 % (found)	Loss = 58.40 % (found)
Cu	Cu
22.57 % (theory)	22.57 % (theory)
25.46 % (found)	26.57 % (found)

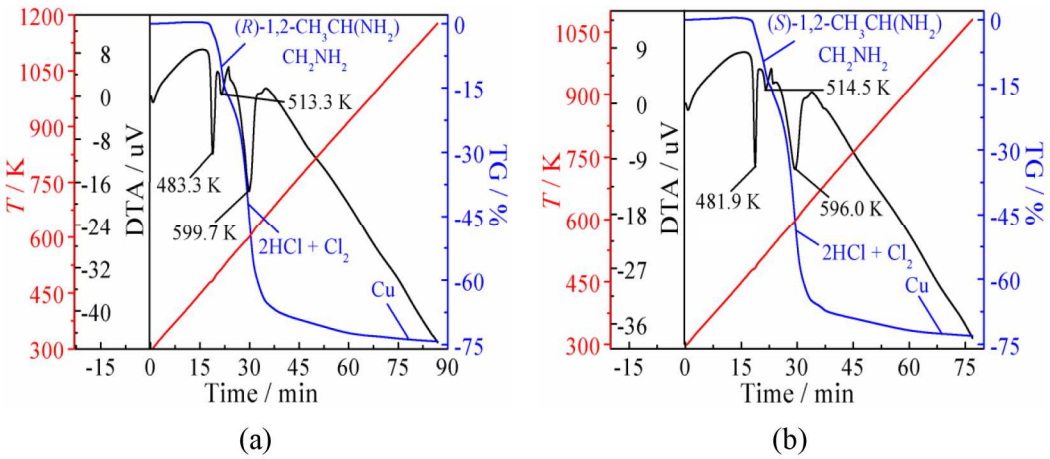

(a) (b)

Figure 5B.2 Thermo gravimetric curves for compounds **18** (a) and **19** (b).

TG/DTA measurements have shown decomposition with the endothermic DTA peak at 483.3 K for compound **18**. Calculated weight lost equivalent to the value for the evaporation of one mole of (*R*)-1,2-diamino propane per formula unit. After the decomposition of (*R*)-1,2-diamino propane, H_2CuCl_4 remain which is very unstable. At higher temperature, above 500 K, it again loses two moles of HCl along with one mole of Cl_2 molecule and in reducing atmosphere of hydrochloric acid so as to convert to Cu. Calculation of second weight loss is equivalent to the evaporation of two moles of HCl and one mole of Cl_2 molecule per formula unit. The remains weight becomes equivalent to the value for copper metal. The decomposition path of compound **18** is very similar to compound **19**. The decomposition path curve for compounds **18** and **19** are shown in Figure 5B.2.

5B.3.4.2 Differential Scanning Calorimetry (DSC)

DSC study on **18** and **19** showed one endothermic transition on their heating and exothermic transition on their cooling. The compounds **18** and **19** showed endothermic transition starting at 404.75 K (-8.77 J g^{-1}) and 404.89 K (-3.93 J g^{-1}) respectively while heating and exothermic transition at 388.71 K (4.36 J g^{-1}) and 389.24 K (1.74 J g^{-1}) respectively while cooling, are characteristic for solid-solid phase transitions as shown in Figure 5B.3. These solid-solid phase transitions are reversible in nature and can be repeated for many cycles without any change in peak position.

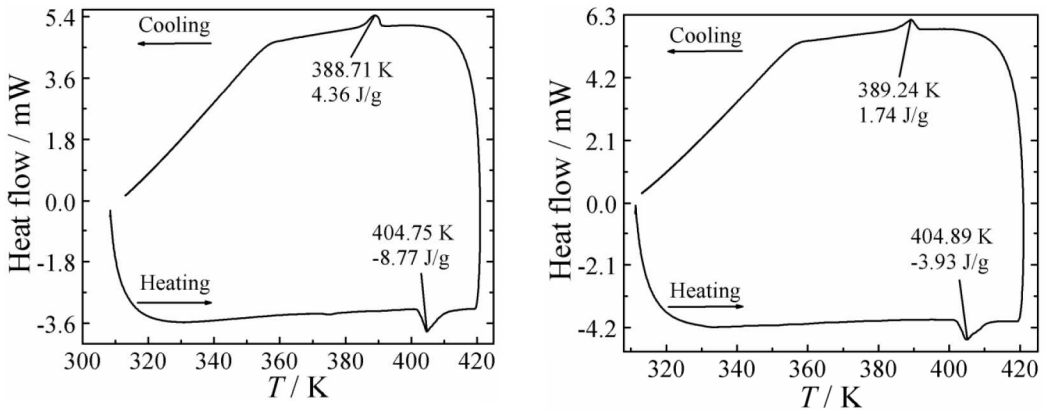

(a) (b)

Figure 5B.3 DSC plots for compounds **18** (a) and **19** (b), at HT showing the reversible transition.

Phase transition observed for compounds **18** and **19** using DSC measurements are correlated to thermochromic behaviors. Indeed, when heated the compound up to there transition temperature in open air, we observed change in color from green ↔ orange for compounds **18** and **19** as shown in Figure 5B.4.

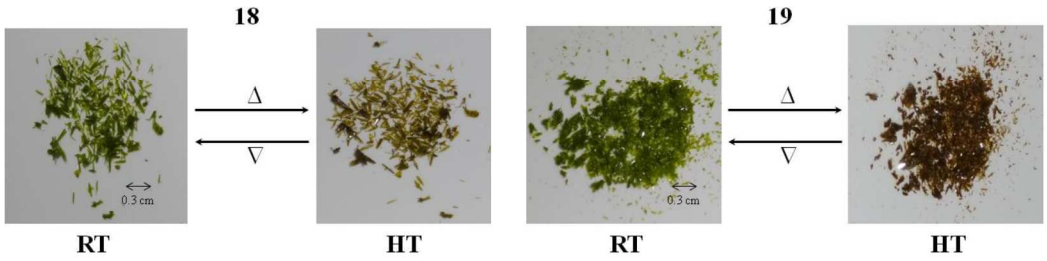

Figure 5B.4 Thermochromic behaviors of crystals for compounds **18** and **19**.

5B.3.5 Crystal Structure

Single crystal XRD infers that compounds **18** and **19** crystallized in orthorhombic chiral space group $P2_12_12_1$. A summary of the crystallographic data collection and refinement parameters for compounds **18** and **19** at 296 K and 150 K are illustrated in Table 5B.1. Figure 5B.5 shows the asymmetric unit consisting of compounds **18'** and **19'**. The dianion of compounds **18** and **19** nearly planar and trans Cl-Cu-Cl angles are in the range of 170.837(15)° - 175.900(19)° at 296 K and 150 K. Protonated hydrogen atoms are apparently located on (*R*)- and (*S*)-1,2-diamino propane and nitrogen atoms are reasonably well ordered as the associated bond distances.

Table 5B.1 Crystallographic data and structure refinement parameters for compounds **18**, **19**, **18'** and **19'**

Compounds	**18**	**19**	**18'**	**19'**
Empirical formula	$C_3H_{12}Cl_4CuN_2$	$C_3H_{12}Cl_4CuN_2$	$C_3H_{12}Cl_4CuN_2$	$C_3H_{12}Cl_4CuN_2$
Formula weight	281.49	281.49	281.49	281.49
T (K)	296(2)	296(2)	150(2)	150(2)
Wavelength (Å)	0.71073	0.71073	0.71073	0.71073
Crystal system	Orthorhombic	Orthorhombic	Orthorhombic	Orthorhombic
Space group	$P2_12_12_1$	$P2_12_12_1$	$P2_12_12_1$	$P2_12_12_1$
a (Å)	7.2200(5)	7.2193(2)	7.1756(3)	7.1744(3)
b (Å)	8.0057(7)	7.9988(3)	7.9615(3)	7.9453(4)
c (Å)	16.0703(11)	16.0683(6)	16.0075(6)	16.0098(7)
β (°)	90	90	90	90
V (Å^3)	928.88(12)	927.88(6)	914.49(6)	912.60(7)
Z	4	4	4	4
D_{calc} (Mg/m^3)	2.013	2.015	2.045	2.049
Crystal size (mm^3)	0.31×0.15×0.10	0.23×0.14×0.12	0.31×0.15×0.10	0.26×0.16×0.13
F(000)	564	564	564	564
2θ range (°)	2.84 - 33.73	2.54 - 33.73	2.54 - 33.72	2.54 - 33.73
Index ranges	-8 ≤ h ≤ 11, -12 ≤ k ≤ 9, -25 ≤ l ≤ 25	-10 ≤ h ≤ 11, -12 ≤ k ≤ 12, -25 ≤ l ≤ 22	-11 ≤ h ≤ 8, -10 ≤ k ≤ 12, -24 ≤ l ≤ 25	-11 ≤ h ≤ 11, -7 ≤ k ≤ 12, -25 ≤ l ≤ 18
Reflections collected	12815	10011	6848	6755
Independent reflections	3674 [R_{int} = 0.0369]	3440 [R_{int} = 0.0323]	3509 [R_{int} = 0.0321]	3320 [R_{int} = 0.0196]
Completeness to θ = 33.73°	99.7 %	99.4 %	99.5 %	99.3 %
Goodness-of-fit on F^2	0.958	0.990	0.847	0.831
Data / restraints / parameters	3674 / 0 / 139	3440 / 0 / 139	3509 / 0 / 139	3320 / 0 / 136
Final R indices [I>2σ(I)]	$R1$ = 0.0243, w$R2$ = 0.0470	$R1$ = 0.0248, w$R2$ = 0.0458	$R1$ = 0.0247, w$R2$ = 0.0474	$R1$ = 0.0179, w$R2$ = 0.0366
R indices (all data)	$R1$ = 0.0307, w$R2$ = 0.0490	$R1$ = 0.0198, w$R2$ = 0.0372	$R1$ = 0.0289, w$R2$ = 0.0493	$R1$ = 0.0333, w$R2$ = 0.0484

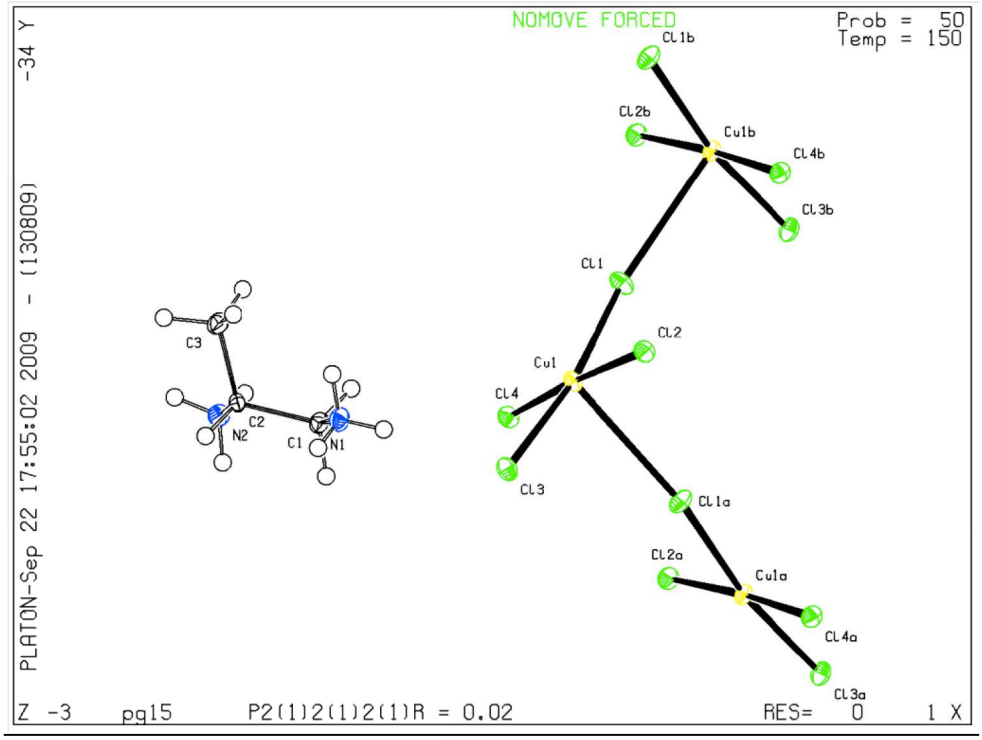

(a)

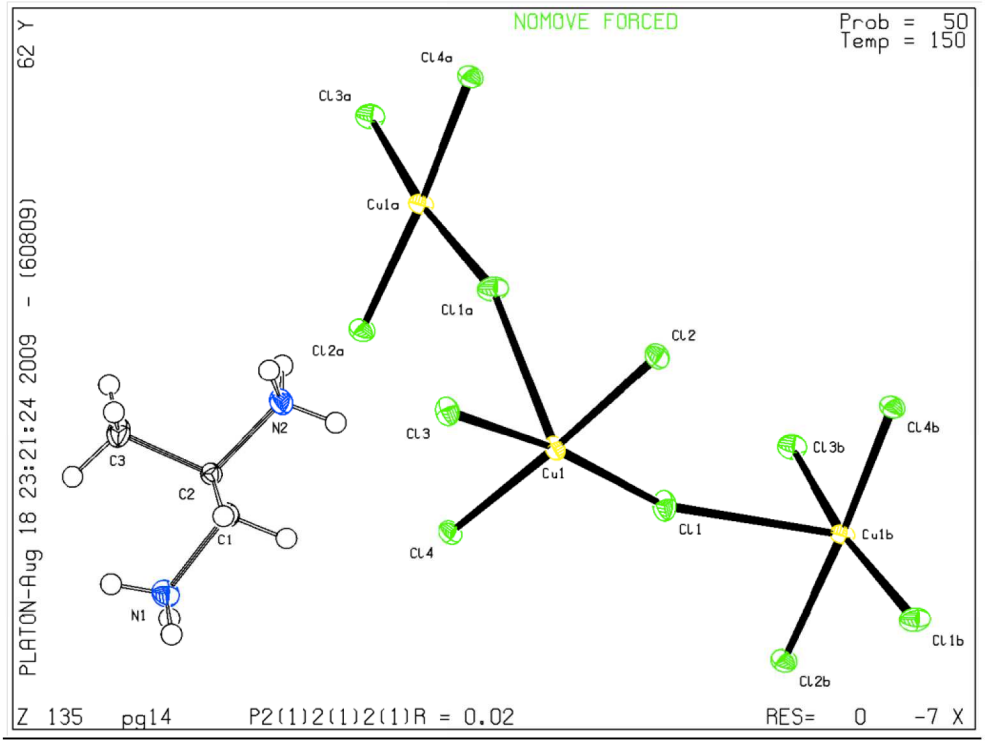

(b)

Figure 5B.5 Molecular view of compounds **18'** (a) and **19'** (b), at 150 K with labeling scheme, displacement ellipsoids are drawn at the 50 % probability level.

The (*R*)- and (*S*)-1,2-diammonium propane copper tetrachloride salts exhibit similar structural features and differ only with respect to the absolute geometry of the diammonium propane cations. Both structures consist of nearly planar $CuCl_4^{2-}$ anions that are weakly hydrogen bonded to the respective diammonium propane cations. The structural parameters associated with the cation are unexceptional. Each of the $CuCl_4^{2-}$ anions is surrounded by mutually interacting four adjacent $CuCl_4^{2-}$ anions. The mean plane passing through the central $CuCl_4^{2-}$ anion is nearly orthogonal (ca. 86°) to the mean planes of each of the four neighboring anions as two mutually trans chloride ligands, namely Cl1 and Cl3, interact with two neighboring $CuCl_4^{2-}$ anions, and the symmetric equivalents of Cl1 and Cl3 belonging to the two remaining $CuCl_4^{2-}$ anions occupy the two axial sites of the central $CuCl_4^{2-}$ anion. This gives an axially distorted octahedral geometry to the copper(II) centers (Figure 5B.6). The inter-anionic Cu···Cl distances are unequal at ca. 2.96 Å and 3.34 Å. The two unique inter metallic Cu···Cu distances are ca. 5.18 Å and 5.61 Å. Two of the chloride ligands are not involved in inter-anionic interactions, and the Cu-Cl distances of these ligands are slightly shorter than the other two Cu-Cl bonds. Both of the ammonium groups of the cation are involved in weak hydrogen bonding interaction with all of the chloride ligands of six neighboring anions with the associated donor-acceptor distances being longer than 3.17 Å Figure 5B.7.

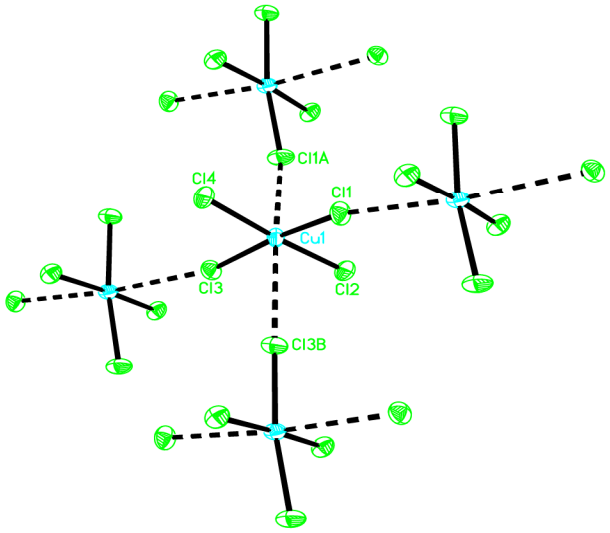

Figure 5B.6 View of the axially interacting $CuCl_4^{2-}$ anions in compound 18 at RT. Except for the atoms of the central octahedron, the rest are unlabeled. Thermal ellipsoids are drawn at 50 % probability and the weak axial bonds are represented by broken bonds.

Unit cell dimensions of the crystals of both salts were determined at 150 K, 225 K and 298 K to determine if they underwent any phase transition. Except for the expected minor expansion of the unit cells due to thermal effects no significant changes were observed as both crystals retain their unit cell dimensions in the 150 K - 298 K temperature range.

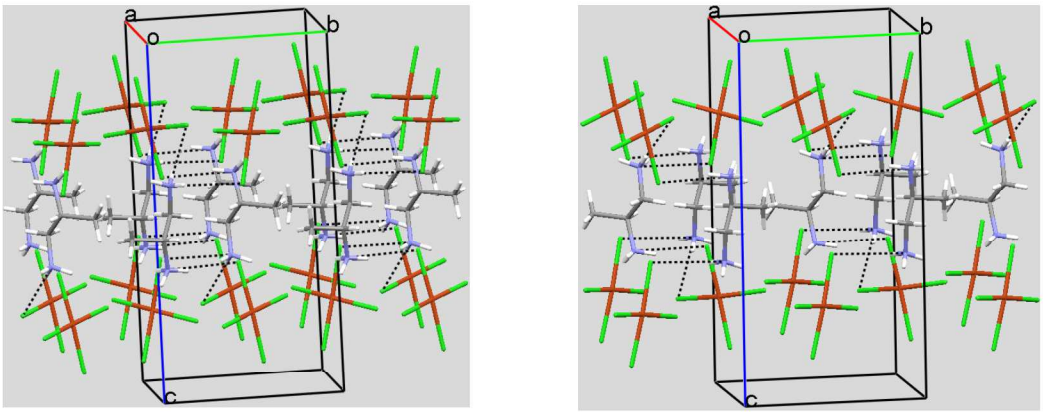

(a) (b)

Figure 5B.7 Orthorhombic structure of compounds **18** (a) and **19** (b), at 296 K viewed along the b-c plane, which showing hydrogen bonding arrangements in oriented organic-inorganic layers.

AT 150 K the isolated $CuCl_4^{2-}$ anions come close together and formed zigzag chains with semicoordinate bond. The average bond angle of bridged Cu-Cl-Cu is 159.75(3)° and average distance of Cu-Cl are 2.29(3) Å for D_S, 3.16(18) Å for D_L at 150 K The chloride atoms in compounds **18'** and **19'** is bonded to the (intralayer) Cu1 ion and Cu1a ion through the bridged coordination mode [Cu1···Cu1a = 5.143(5) Å]. But there is no change in space group of the crystal system at 150 K. Thus in effect, better geometry is specified as 4+1+1 or 4+1 coordination and the layers are nearly sliced in $(CuCl_4^{2-})_n$ zigzag chain running parallel to the *a*-axis at 150 K as illustrate in Figure 5B.8. The extreme elongation of the one semicoordinate bond allowed the accommodation of chiral enantiomers (*R*)- and (*S*)-1,2-diammonium propane cations between the zigzag chains. The ammonium groups needs to be able to fit into the "holes" formed by terminal and bridging halogen within the layers, without the rest of the molecule interfering with the sheets. The ammonium heads of OACs N(2) at 296 K hydrogen bonded by only one terminal chlorine and N(1) bonded by bifurcated hydrogen bonds to two chlorine (one free and one terminal) leading to shift of a perfectly eclipsed configuration [6]. At 150 K both ammonium heads of OACs

bonded by bifurcated hydrogen bond to two chlorine (one free and one terminal), resulted in shifting of a perfectly eclipsed configuration. Figure 5B.7 and 5B.8, represented that the ammonium group of OACs hydrogen bonded to terminal chlorine whose position always tilts the $CuCl_4^{2-}$ along the axis and bonding with bridging chlorine always forcing the alternating layer chlorine atoms out of the plane, leading to causes tilt of the inorganic layers. The atoms of (*R*)- and (*S*)-1,2-diammonium propane cation lie on general positions. The cation backbone is not planar, with N(1)-C(1)-C(2)-C(3) bond assuming the gauche conformation with torsion angle -65.15(16)° and N(1)C(1)-C(2)-N(2) is also not planer having torsion angle 173.77(12)° that exhibits trans-staggered conformation has an important impact for hydrogen-bonding scheme. Whereas hydrogen atoms at both end of the ammonium heads in hydrogen bonding scheme have "trans-staggered" conformation using free chlorine and "gauche-eclipsed" conformation using terminal chlorine. While the hydrogen atoms of the ammonium heads in (*R*)- and (*S*)-1,2-diammonium propane cations which are located both sides of the inorganic layers have "gauche-eclipsed" conformation using free chlorine and have "trans-staggered" conformation using terminal chlorine with important impact on the hydrogen bonding scheme. Hydrogen bonds and their angles are defined in Table 5B.2. Thus, the $-NH_3^+$ group of (*R*)- and (*S*)-1,2-diammonium propane cation formed bifurcated hydrogen bond with two chlorine (one free and one terminal) and with two zigzag chain in the plane. A variety of interactions are responsible for stabilizing the layered structures.

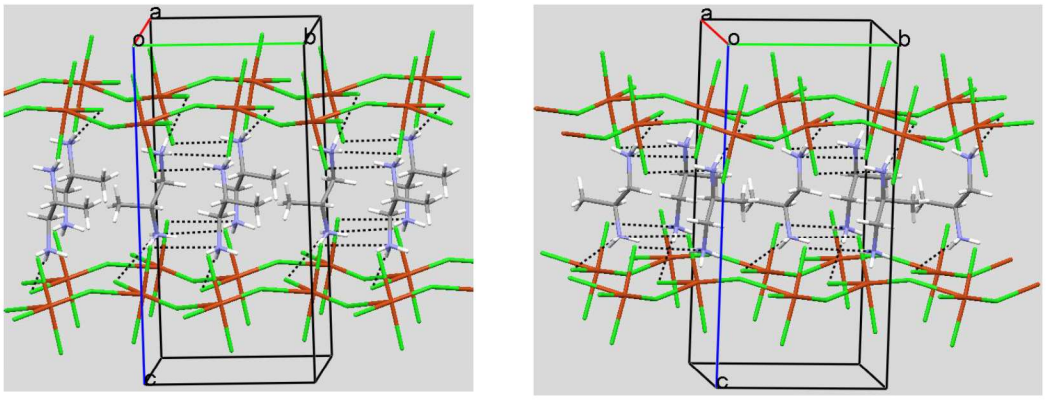

(a) (b)

Figure 5B.8 Orthorhombic structure of compounds **18** (a) and **19** (b), at 150 K view along b-c plane, which reveal hydrogen bonding arrangements between chlorine and $-NH_3^+$ group and zigzag chain layers structure of $CuCl_4^{2-}$ and their stability.

Table 5B.2 Hydrogen bonds and angles for OIHCs [Å and °]

Compounds	Cu-Cl [Å]	Cu-Cu Dist. [Å] Inter	Cu-Cu Dist. [Å] Intra	Cl-Cl Dist. [Å] Terminal	Cl-Cu-Cl Angle[°]	N···Cl Dist. [Å]	N-H···Cl Angle[°]
18	2.3201(5)	8.0448(6)	5.1791(4)	3.6489(5)	175.900(19)	3.3524(19)	144(3)
	2.2979(5)				170.95(2)	3.2260(19)	118(3)
	2.2699(4)				91.289(16)	3.470(2)	134(3)
	2.2587(4)				90.427(17)	3.6103(19)	130(2)
					89.642(16)	3.2734(18)	166(3)
					89.274(16)	3.1829(17)	167(2)
						3.3090(18)	171(3)
						3.395(2)	141(3)
						3.5338(18)	135(3)
19	2.3185(5)	8.0438(4)	5.1768(3)	3.6477(6)	175.905(18)	3.3494(19)	143(3)
	2.2959(5)				171.024(19)	3.466(2)	137(3)
	2.2696(5)				91.288(17)	3.222(2)	113(2)
	2.2590(4)				90.427(18)	3.3494(19)	143(3)
					89.643(17)	3.2771(19)	168(3)
					89.267(17)	3.1824(19)	164(3)
						3.3106(18)	167(3)
						3.3905(18)	139(3)
						3.5296(18)	137(3)
18'	2.3168(5)	8.0132(4)	5.1464(3)	3.6181(6)	175.632(18)	3.3191(17)	143(3)
	2.2978(5)				170.843(18)	3.2008(18)	121(2)
	2.2692(5)				91.327(16)	3.4352(18)	131(2)
	2.2599(5)				90.419(17)	3.5720(18)	135(2)
	2.9253(4)				89.594(16)	3.2453(17)	173(3)
					89.343(16)	3.1668(17)	162(2)
						3.2832(17)	170(2)
						3.3595(18)	140(2)
						3.5114(17)	138(2)
19'	2.3146(4)	8.0143(4)	5.1400(3)	3.6184(2)	175.612(14)	3.4319(14)	136(2)
	2.2949(4)				170.837(15)	3.3161(14)	151(2)
	2.2692(3)				91.306(12)	3.5656(13)	129.4(16)
	2.2603(3)				90.470(12)	3.2416(12)	172(2)
	2.9253(4)				89.637(12)	3.2827(13)	169.9(18)
					89.272(12)	3.1618(14)	157.3(16)
						3.3546(13)	145(2)
						3.5047(13)	129.2(18)

In these systems, the inorganic layer is separated by monolayer of organic ammonium cations. These organic cations are hydrogen bonding to the inorganic layer at both ends rather than only one end and removing van der Waals gap between the layers. Therefore, copper atoms are in one layer almost directly over those in the adjacent layers and providing for the possibility of substantial interaction between the

layers through interlayer terminal Cu-Cl···Cl-Cu pathway. The interlayer Cl···Cl distance for compounds **18** and **19** are 3.648(2) Å and 3.618(2) Å at 296 K and at 150 K, which is close to 0.048 Å to 0.018 Å greater than sum of the van der Waals radii. Therefore, the interlayer distance appeared to be primarily dictated by the length of OACs rather than by halide-halide repulsion [7]. The bond distances and angles for OIHCs are given in the Table 5B.2.

CCDC No. 817862 and 817864 contains the crystallographic data for the compounds **18** and **19**. These data can be obtained free of charge via http://www.ccdc.cam.ac.uk/conts/retrieving.html, or from the Cambridge Crystallographic Data Centre, 12 Union Road, Cambridge CB2 1EZ, UK; fax: (+44) 1223 336 033; or e-mail: deposit@ccdc.cam.ac.uk.

5B.3.6 Magnetic Properties

Magnetic susceptibility measurements were obtained by Quantum Design SQUID magnetometer. This magnetometer works between 1.8 K and 300 K for direct current (dc) applied fields ranging from -7 to +7 Tesla (T). Figure 5B.9 (a) and (b) shows the temperature-dependent molar magnetic susceptibility of chiral polycrystalline compounds **18** and **19** in the temperature range 2 K - 300 K. At 300 K χT values are 0.404 cm^3 K mol^{-1} (1.8 μ_B) at 1000 Oe [greater than expected 0.375 cm^3 K $mole^{-1}$ (1.73μ_B) for Cu^{2+} ions] and χT values are found nearly constant till 100 K. The χT values gradually decreases with decreasing temperature and reaches a minimum at 20 K. On further cooling the χT values increases abruptly to a peak at 19 K and then sharply falls to 0.031 cm^3 K mol^{-1} (0.50 μ_B) and 0.018 cm^3 K mol^{-1} (0.38 μ_B) at 2 K for compounds **18** and **19** respectively. This type of magnetic behavior is characteristic of canted antiferromagnetism as reported extensively before [8]. The final decrease of the χT value indicates the presence of intermolecular interaction and/or magnetic anisotropy of Cu (II) ions [9]. The field-cooled (FC) and zero-field-cooled (ZFC) susceptibility $\chi(T)$ are measured at 300 Oe (Figure 5B.9 inset shown as χ versus T plots). The FC and ZFC susceptibility at 19 K confirmed the long-range magnetic ordering. The peak at 19 K in the FC and ZFC curve are corresponding to the Neél temperature, a critical temperature for the antiferromagnetic long-range order. The temperature dependence of the magnetic susceptibility at various field are shown in

Figure 5B.10. At the low field χT values gradually decreased upon cooling and reached minimum at 20 K upon further cooling. The χT values increased to maximum at 19 K then decreased at 2 K, reflecting dominant intra chain antiferromagnetic interactions. But when applied fields are stronger, the antiferromagnetism region become weaker and disappears. Such behavior suggested the existence of some field-induced spin canting which results in magnetic interactions changing form an antiferromagnetic to ferromagnetic state. While in χ versus T curves after reaching a broad maximum (χ_{max} = 0.0085 $cm^3\ mol^{-1}$) at 25 K decreased slightly with decreasing the temperature till 20 K, then abruptly increased upon further cooling to a peak at 19 K which decreased slowly and again increased continuously up to 2 K. The sharp peak at 19 K indicated the occurrence of a long-range ordering below the 20 K and below the 10 K reflects weak ferromagnetic ordering. In low applied fields $\chi(T)$ has shown a peak at 19 K which becomes weaker and disappears when the applied field is high. For the external field, width of antiferromagnetism region reached maximum when H = 100 Oe. The region of antiferromagnetic is narrow and state below 9 K mostly in weak ferromagnetic. It seems that when applied fields are stronger antiferromagnetism region becomes weaker and disappears. Which overcomes the inter chain antiferromagnetic interaction and field-induced magnetic transition from an antiferromagnetic to a ferromagnetic state.

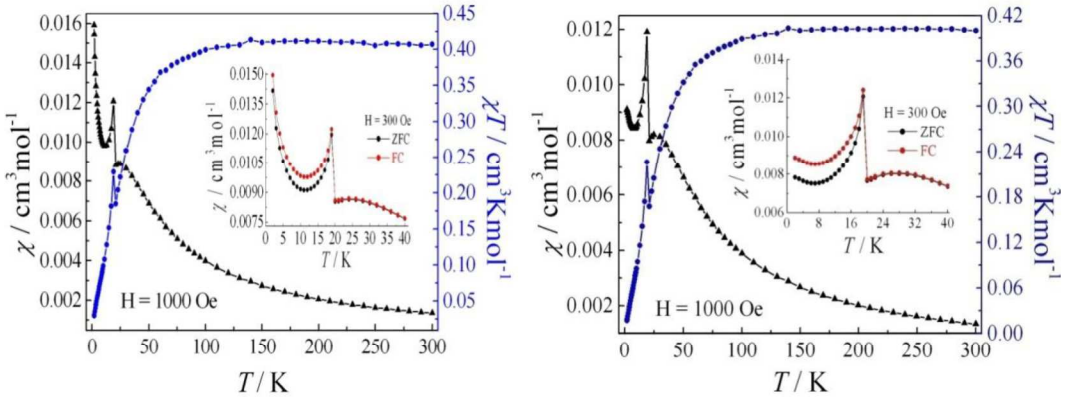

Figure 5B.9 The temperature dependent χ and χT plots on polycrystalline compounds **18** (a) and **19** (b), at 1000 Oe, FC and ZFC susceptibility plots at 300 Oe (inset).

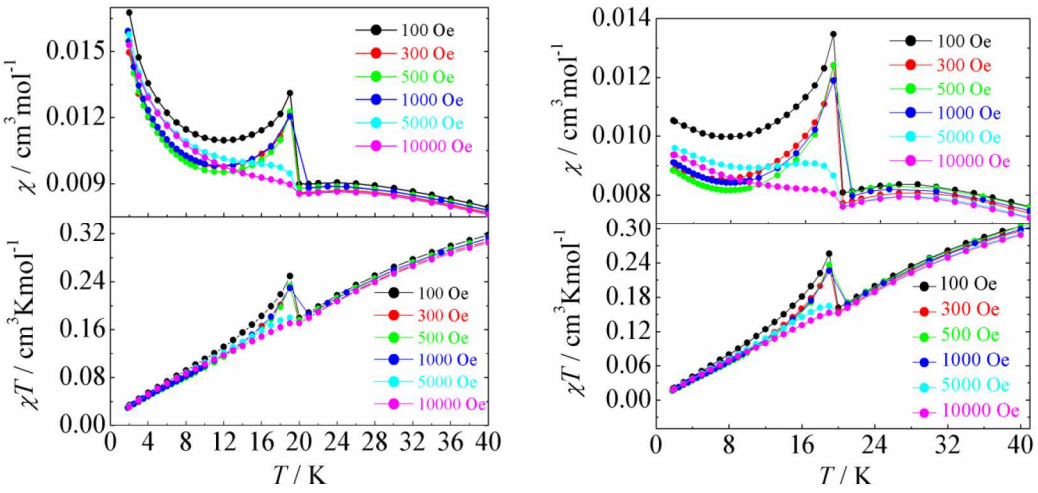

Figure 5B.10 The temperature dependence χ (above) and χT (below) plots for compounds **18** (a) and **19** (b), at different applied magnetic fields.

As shown in Figure 5B.11 (a), χ^{-1} versus T plot in the temperature range 40 K - 300 K, the susceptibility data above 182 K are well-fitted and obeys the Curie-Weiss law gives straight line with C = 2.51(5). The intercept with T axis yields positive θ = 5.6 K and 3.93 K for compounds **18** and **19** respectively. The positive θ values indicate the presence of weak ferromagnetic interaction. The field dependence of M versus (H) curve for compounds **18** and **19** was taken at 2 K, where M = dc magnetization and H = magnetic field. The magnetization at 2 K increased gradually with H, as a typical antiferromagnet and then increased slightly rapidly above 2000 Oe [Figure 5B.11 (b)] for compound **19**. Above the 6000 Oe it increased slowly again, reached a value of 4 × 10^{-2} (emu) at 64000 without reaching a saturation magnetization value $M_S = N\beta gS$ (where S = spin associated with the molecular ground state and g = Zeeman factor). The shape of M versus H plot at 2 K suggests the presence of metamagnetic behavior [8,10].

To confirm this long range ordering ac-susceptibility measurements for both compounds were carried out. The ac-susceptibility measurements at zero applied dc field and at 997 Hz frequency [in-phase (real) ac magnetic susceptibility (χ') and out-of-phase (imaginary) ac-susceptibility (χ'')] are shown in Figure 5B.12. The in-phase (χ') as well as out-of-phase (χ'') are not giving any information in temperature range 2 K - 24 K for compounds **18** and **19**.

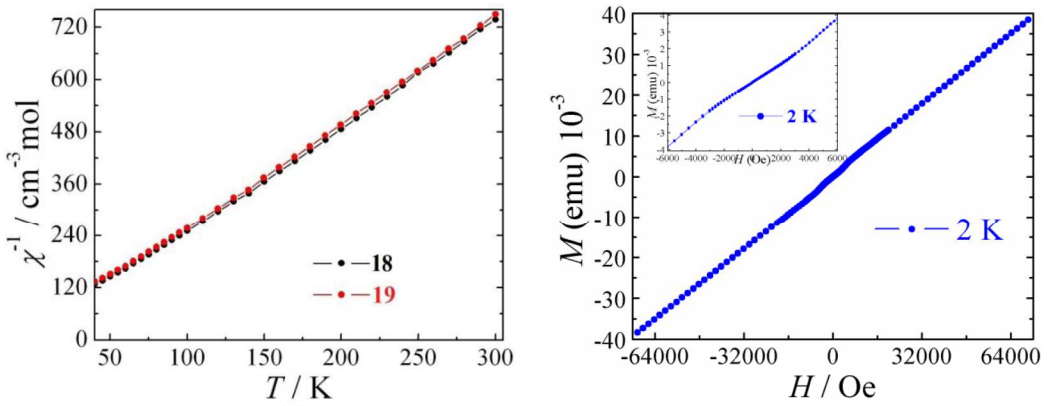

Figure 5B.11 The χ^{-1} versus T plot for compounds **18** and **19** and *M*-*H* plots for compound **19** measured at 2 K.

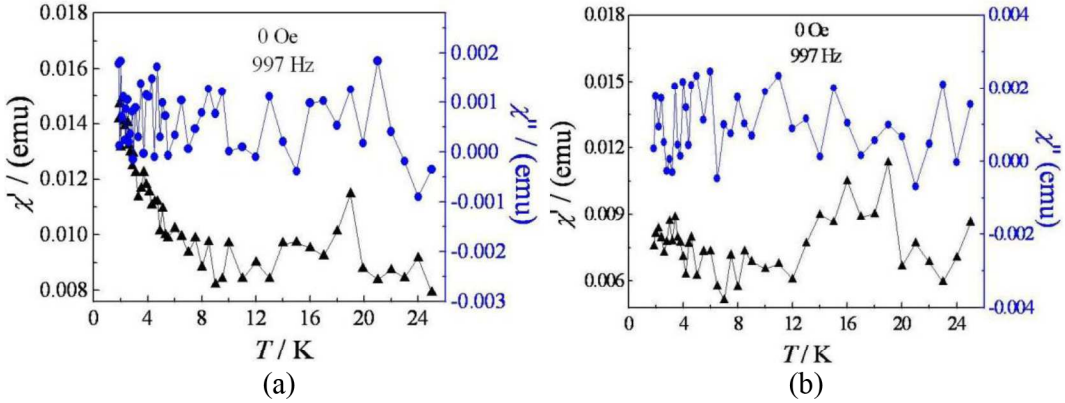

Figure 5B.12 The temperature variation ac-susceptibility plots real (χ') (a) and imaginary (χ'') (b), for compounds **18** and **19** at 997 Hz.

5B.4 Conclusion

- We have synthesized yellow-green color shining rectangular prism like crystal of layered OIHCs, [(*R*)- and (*S*)-1,2-diammonium propane]$CuCl_4$, by using chiral diammonium salts.
- Thermal studies for compounds **18** and **19** showed reversible solid-solid phase transitions at 404.75 K and 404.89 K on heating and at 388.71 K and 389.24 K on their cooling.
- The solid-solid phase transitions (compounds **18** and **19**) above the room temperature responsible for change in color from green ↔ orange (thermochromic behavior).

- Single crystal XRD measurements for compounds **18** and **19** have shown it crystallized in orthorhombic chiral space group $P2_12_12_1$.
- At 296 K $CuCl_4^{2-}$ anions have isolated distorted square-planar geometry, while at 150 K it adopts distorted square-pyramidal geometry and formed zigzag chains with semicoordinate bond for compounds **18** and **19**.
- The magnetic properties by SQUID magnetometer measurements displayed field-induced metamagnetic properties and has shown an antiferromagnetic long-range ordering with T_N of 20 K for compounds **18** and **19**.

References

[1] G. B. Birrell, B. Zaslow, *J. Inorg. Nucl. Chem.* **1972**, *34*, 1751.

[2] D. W. Phelps, D. B. Losee, W. E. Hatfield, D. J. Hodgson, *Inorg. Chem.* **1976**, *15*, 3147-3152.

[3] L. O. Snively, P. L. Seifert, K. Emerson, J. E. Drumheller, *Phys. Rev. B* **1979**, *20*, 2101-2104.

[4] H. R. Wen, Y. Z. Tang, C. M. Liu, J. L. Chen, C. L. Yu, *Inorg. Chem.* **2009**, *48*, 10177-10185.

[5] E. K. Gibson, J. M. Winfield, K. W. Muir, R. H. Carr, A. Eaglesham, A. Gavezzotti, D. Lennon, *Phys. Chem. Chem. Phys.* **2010**, *12*, 3824-3833.

[6] M. J. Riley, D. Neill, P. V. Bernhardt, K. A. Byriel, C. H. L. Kennard, *Inorg. Chem.* **1998**, *37*, 3635-3639.

[7] G. Amirthaganesan, M. A. Kandhaswamy, M. Dhandapani, *Cryst. Res. Technol.* **2007**, *42*, 684-687.

[8] K. C. Mondal, G. E. Kostakis, Y. Lan, C. E. Anson, A. K. Powell, *Inorg. Chem.* **2009**, *48*, 9205-9213.

[9] X. -N. Cheng, W. -X. Zhang, X. -M. Chen, *J. Am. Chem. Soc.* **2007**, *129*, 15738-15739.

[10] P. Yin, S. Gao, L. -M. Zheng, Z. Wang, X. -Q. Xin, *Chem. Commun.* **2003**, 1076-1077.